MARMARA UNIVERSITY
INSTITUTE FOR GRADUATE STUDIES
IN PURE AND APPLIED SCIENCES

SYNTHESIS OF CHITOSAN-BASED BIOCOMPATIBLE CONDUCTIVE POLYMER FOR BIOSENSOR APPLICATIONS

CELİL ULUTÜRK

MASTER THESIS
Department of Chemical Engineering

Thesis Supervisor
Asst. Prof. NESLİHAN ALEMDAR

ISTANBUL, 2016

MARMARA UNIVERSITY
INSTITUTE FOR GRADUATE STUDIES
IN PURE AND APPLIED SCIENCES

SYNTHESIS OF CHITOSAN-BASED BIOCOMPATIBLE CONDUCTIVE POLYMER FOR BIOSENSOR APPLICATIONS

CELİL ULUTÜRK

(524512004)

MASTER THESIS
Department of Chemical Engineering

Thesis Supervisor
Asst. Prof. NESLİHAN ALEMDAR

ISTANBUL, 2016

ACKNOWLEDGEMENT

I owe a dept to many people who help me during my master thesis studies. Firtly, i would like to state my sincere thankfullness to my advisor Asst. Prof. Neslihan ALEMDAR for her motivation, and extensive knowledge. She allowed this paper to be my own work, but steered me in the right the direction whenever she thought I needed it.

Beside my advisor, I would like to thank the Prof. Atıf KOCA and his friends for their helps.

I would also like to thank Marmara University Scientrific Research Project Coordination Unit (BAPKO) for the financial support and Institute for Graduate Studies in Pure and Applied Sciences, Marmara University for their elegant education system.

At last, i must express my very deep thankfullness to my mother, my father and my sister for their endless support and continuous encouragement through the process of researching and writing this thesis. A heartfelt thanks also goes out to Elif ÇETİNKAYA for all her love and endless support. This accomplishment would not have been possible without them.

LIST OF CONTENTS

ABSTRACT

SYNTHESIS OF CHITOSAN-BASED BIOCOMPATIBLE CONDUCTIVE POLYMER FOR BIOSENSOR APPLICATIONS

Electroconductive hydrogels are multifunctional smart materials that combine a three-dimensional hydrated polymeric structure with the electrical conductivity. In this study, by using two different methods, chitosan-based-electroconductive hydrogel was fabricated for biomedical applications.

In the first approach to produce conductive hydrogel, glycidyl methacrylate (GMA) was grafted on the chitosan backbone to form CTS-g-GMA product. Then, a variety amounts of reduced graphene oxide (RGO) (from 0% to 15%) were encapsulated into the polymeric network forming CTS-g-GMA and poly(ethylene glycol)diacrylate (PEGDA) by using photo-crosslinking technique. In the second approach, polyaniline solution prepared by utilizing different concentrations of aniline (0.08, 0.16 and 0,32M) was absorbed into (CTS-g-GMA)-PEGDA crosslinked structure. The structures of hydrogels were confirmed by XRD and FTIR analysis. Thermal performances of the conductive hydrogels were examined by TGA. Water uptake capacity of hydrogels determined gravimetrically. L929 fibroblast cells were used for cytotoxicity test. Conductivity of the hydrogel was determined by four-point probe technique. Thermal analyses showed that RGO content was improved thermal stability of hydrogels. According to conductivity measurements; the highest conductivity (1.716×10^{-3} S/cm) was obtained when 10% RGO was encapsulated into the polymeric structure. For polyaniline-chitosan based hydrogel, TGA results demonstrated that PANI chains in [(CTS-g-GMA)-PEGDA] reduced the thermal stability of the hydrogels. Among the PANI-based hydrogels, [(CTS-g-GMA)-PEGDA]-PANI(0.32M) has the highest conductivity value ($7{,}437 \times 10^{-3}$ S/cm).

All the obtained results showed that both hydrogels fabricated in this study are promising candidates for biomedical applications especially biosensors owing to their outstanding advantages.

ÖZET

BİYOSENSÖR UYGULAMALARI İÇİN KİTOSAN BAZLI BİYOUYUMLU İLETKEN POLİMER SENTEZİ

İletken hidrojeller üç boyutlu hidrate polimerik yapı ile elektriksel iletkenliği birleştiren çok fonksiyonlu akıllı malzemeleredir. Bu çalışmada, iki farklı metot kullanılarak biomedikal uygulamalarda kullanılabilecek kitosan bazlı iletken hidrojeller üretilmiştir.

İletken hidrojel üretimi için uygulanan ilk yöntemde; kitosan ana zinciri üzerine glisidil metakrilat (GMA) aşılandı ve böylece CTS-g-GMA ürünü elde edildi. Daha sonra, çeşitli miktarlarda indirgenmiş grafen oksit (RGO) (%0'dan %15'e kadar), CTS-g-GMA ve poli(etilen glikol)diakrialat (PEGDA)'ın ışınlanma ile çapraz bağlanmasıyla oluşturulan polimerik ağ içerisine enkapsüle edildi. İkinci yaklaşımda ise, farklı konsantrasyonlarda anilin (0.08, 0.16 ve 0.32M) kullanılarak hazırlanan polianilin çözeltileri çapraz bağlı (CTS-g-GMA)-PEGDA yapının içerisine absorbe ettirildi. Her iki yöntem ile elde edilen hidrojellerin yapıları FTIR ve XRD analizleri ile doğrulandı. Hidrojellerin su alma kapasitesileri gravimetrik yöntem kullanılarak hesaplandı. L929 fibroblast hücreleri sitotoksisite testleri için kullanıldı. Hidrojellerin iletkenlikleri ise dört-nokta prob metodu ile belirlendi. Termal analiz sonuçları RGO içeriğinin hidrojellerin termal kararlılığını arttırdığını göstermiştir. İletkenlik ölçümleri sonuçlarına göre, en yüksek iletkenlik (1.716×10^{-3} S/cm) değeri, polimerik yapı içerisine %10 oranında RGO'nun enkapsülasyonuyla elde edilmiştir. Polianilin-kitosan bazlı hidrojel için yapılan TGA sonuçları, [(CTS-g-GMA)-PEGDA] içindeki polianilin zincirlerinin hidrojelin termal kararlılığını düşürdüğünü göstermiştir. Belirlenen iletkenlik değerleri kıyaslandığında PANI bazlı hidrojeller arasında, [(CTS-g-GMA)-PEGDA]-PANI(0.32M) hidrojelinin en yüksek iletkenlik değerine ($7{,}437 \times 10^{-3}$ S/cm) sahip olduğu gözlemlenmiştir.

Bu çalışmada elde edilen sonuçlara göre, her iki yöntemle de üretilen üstün avantajlara sahip bu hidrojellerin biyomedikal alanlarda özellikle de biyosensör uygulamalarında kullanılabileceği öngörülmektedir.

SYMBOLS

I	: Current	(A)
s	: Probe Space	(m)
V	: Voltage	(V)
Ws	: Swollen mass of hydrogel	(kg)
Wd	: Dry mass of hydrogel	(kg)
σ	: Conductivity	$(S \cdot m^{-1})$
ρ	: Sheet resistivity	$(\Omega \cdot m)$

ABBREVIATIONS

2-D	: Two-dimensional
3-D	: Three-dimensional
APS	: Ammonium peroxodisulfate
C_2H_3N	: Acetonitrile
$C_6H_5NH_2$	: Aniline
CH_3COOH	: Acetic acid
CP	: Conducting polymer
CTS	: Chitosan
DTA	: Differential thermal analysis
DMEM	: Dulbecco's Modified Eagle Medium
ECH	: Electroconductive Hydrogel
EtOH	: Ethanol
FTIR	: Fourier Transform Infrared
g	: graft
GMA	: Glycidyl methacrylate
GO	: Graphene oxide
H_2O_2	: Hydrogen peroxide
H_2SO_4	: Sulfuric acid
HA	: Hyaluronic acid
HCl	: Hydrochloric acid
KNO_3	: Potassium nitrate
KOH	: Potassium hydroxide
PANI	: Polyaniline
PEDOT	: Poly(3,4-ethylenedioxythiophene)

PEGDA	: Poly(ethylene glycol) diacrylate
PGMA	: Poly(glycidyl methacrylate)
PPy	: Polypyrrole
RGO	: Reduced graphene oxide
TGA	: Thermogravimetric analysis
THF	: Tetrahydrofuran
SWNT	: Single-walled carbon nanotubes
UV	: Ultraviolet
WST-1	: 4-[3-(4-iodophenyl)-2-(4-nitrophenyl)-2H-5-tetrazolio] 1,3benzenedisulfonate
XRD	: X-Ray Diffraction

LIST OF FIGURES

LIST OF TABLES

1 INTRODUCTION

1.1 Hydrogels

Hydrogels, which consist of three dimensional (3-D) polymeric networks, are known as their good water absorption ability, soft and rubbery consistency. They are water-insoluble owing to crosslinks in network structure and hydrophilic functional groups that, bound to water molecules by hydrogen bonds, are gained water absorption ability [1]. When the water enters the hydrogel matrix, the polar hydrophilic groups in the network are hydrated firstly. This forms primary bound water. In this way, network structure expands and exposing hydrophobic sides of the chains interact with water molecules. These called as secondary bound water and these two types of bound waters so called as total bound water. Polymer matrix is filled with free water expect for bound water. After the interactions of water molecules with hydrophobic and hydrophilic groups, meshes full additional water owing to osmotic driving force and this water called as free water. Crosslinks exhibit a retraction force against to this extra swelling. This establishes an equilibrium swelling level and hinders the deformation of hydrogel [2].

The classification of hydrogels can be done based on various points like according to their resources (natural hydrogels and synthetic hydrogels), polymeric composition (homopolymeric hydrogels, copolymeric hydrogels, multipolymer interpenetrating polymeric hydrogels), configuration (amorphous hydrogels, semicrystalline hydrogels, crystalline hydrogels), electrical charge (Nonionic hydrogels, ionic hydrogels, amphoteric hydrogels, polybetaines hydrogels). But hydrogels are broadly classified based on type of crosslinking. Crosslinking can be formed chemically or physically. [1].

1.1.1 Physical Hydrogels

Physicochemical interactions such as hydrophobic interactions, hydrogen boding, stereocomplexation, supramolecular chemistry and electrostatic ionic force keep together chains and form the physical hydrogels. These reversible interactions stand against to the dissolution of the hydrogels [3]. Polymer chains can interact simultaneously or an external stimulant can start the physical interactions such as sound, light, pressure, pH, heat, electric signal [4]. Physically crosslinked hydrogels can form

by charge interactions between two polymers or between a small molecule and a polymer of opposite charge (Figure 1.1). Physical Hydrogels formed by charge interactions can degrade biologically cause of the some ionic species in the body. Furthermore, formation or degradation of crosslinks can be launch by changes in pH [5,6].

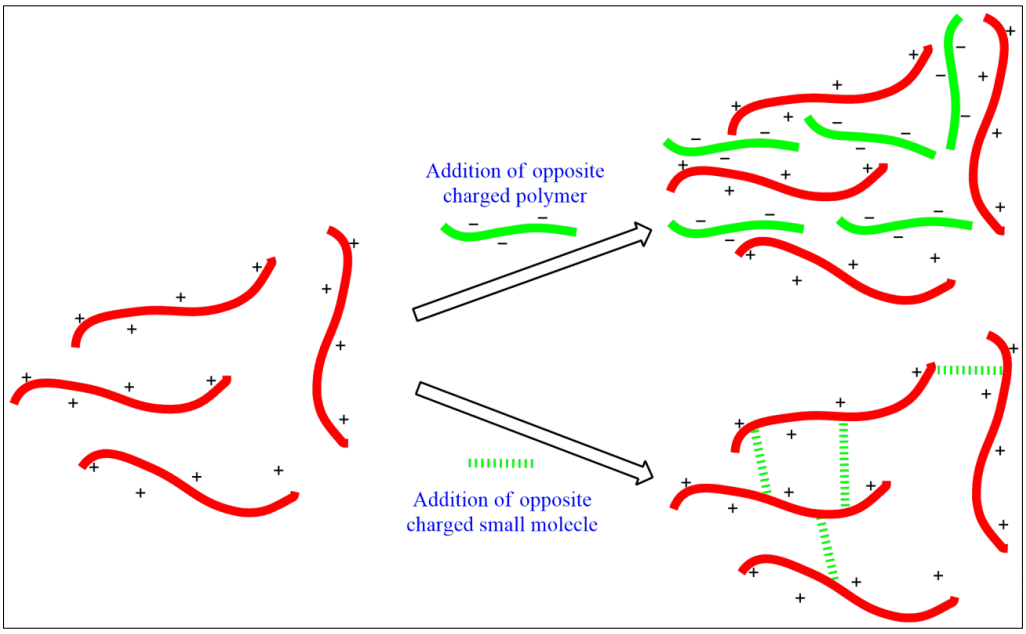

Figure 1.1 Formation of physical hydrogels via charge interactions

Hydrophobic segments of amphiphilic copolymers (graft and block copolymers) can crosslink each other in aqueous media to form hydrogels (Figure 1.2). This crosslinking occurs with reverse thermal gelation. Hydrophobic segments combine by increasing temperature for minimizing the hydrophobic part of the polymer chains interacted with water, decreasing the water amount interacting with the hydrophobic parts and maximizing the solvent entropy [5,6]. Another physical interaction to obtain hydrogels is hydrogen bonds between polymers. Injectable hydrogels can be produced thanks to hydrogen bonds. If two or more natural polymers are mixed, the polymer blends may exhibit gel like behavior compared to the individual components. This synergistic effect is provided by hydrogen bods between polymer chains. However, shearing forces can break the weak hydrogen bonds. Starch-carboxymethyl cellulose and hyaluronic acid-

methylcellulose natural polymer blends are examples that having capacity for formation injectable hydrogels by hydrogen bonding [5].

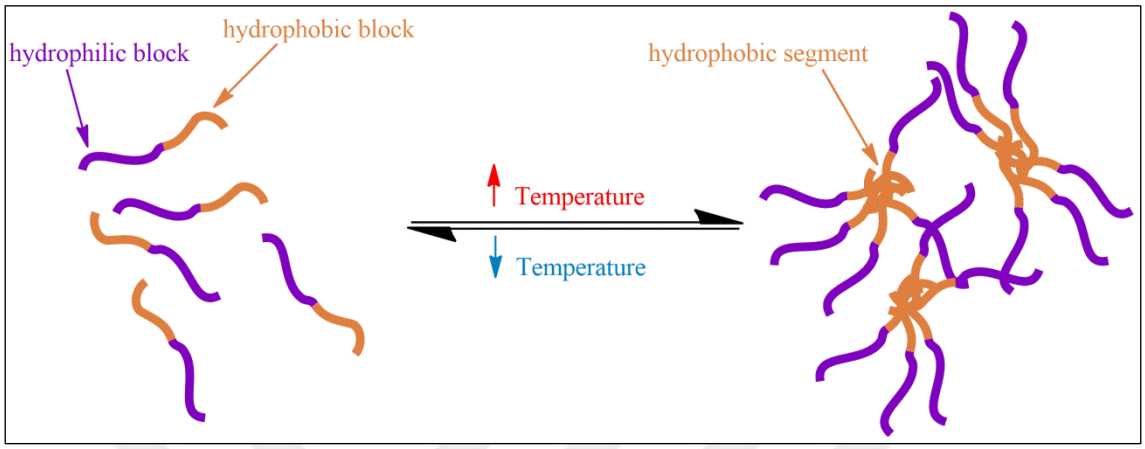

Figure 1.2 Formation of physical hydrogels by hydrophobic interactions

A further strategy for forming physically crosslinked hydrogels is stereocomplexation. Some stereoisomer polymers can compose an intermolecular complex (stereocomplex). Various kinds of polymer pairs can be used to obtain the stereocomplexes, L-lactide and D-lactide are expressed as a well-known example [4,5].

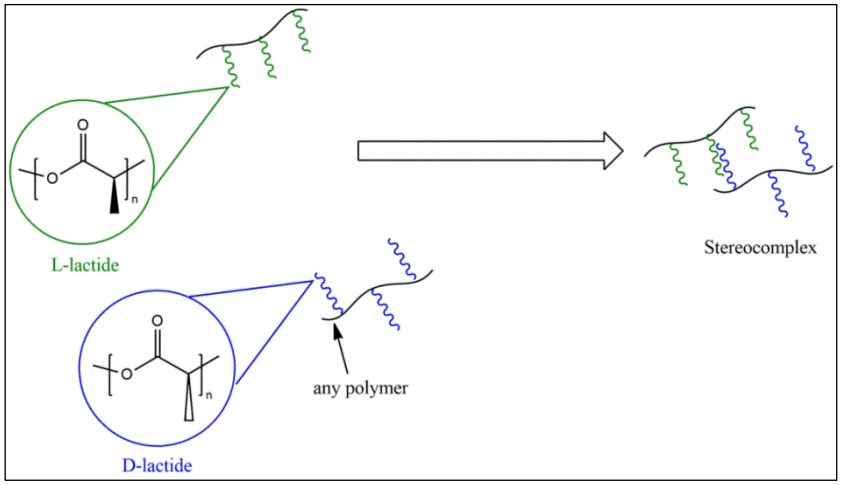

Figure 1.3 Stereocomplexation between L- and D- lactide polymer chains

1.1.2 Chemical Hydrogels

The polymer chains are connected each other by covalent bonds to form a chemical hydrogel in a 3-D polymer network. Therefore, chemical hydrogels have higher mechanical strength and longer degradation time than physical hydrogels. Various kinds of methods are used to synthesize chemical crosslinked hydrogels [5,7]. Reaction of pendant hydrophilic functional groups (OH, COOH and NH_2) by means of high energy radiation (electron beam and gamma rays), usage of enzymes and radical polymerization of vinyl monomers or macromonomers are strategies of chemical hydrogel synthesis [6,7]. In this study, photo-crosslinking technique was preferred cause of the advantages such as low energy requirement, no volatile organic compounds release, in situ gelation, rapid and controllable reaction. Some characteristic features of the hydrogels such as swelling capacity, structural and morphological properties can be modified by regulating the photoinitiator concentration, ultraviolet (UV) exposure time, UV light intensity, molar ratios of monomers and/or polymers. Moreover, the UV photo-crosslinking processes can allow the formation of the hydrogel in any desired pattern. Photo-crosslinked hydrogels are ideal materials for biomedical applications cause of all these factors. In this method, aqueous solution of polymers contained photoinitiator is exposed to UV irradiation and absorbed UV light by this initiator causes generating free radicals which catalyzing the polymerization and/or crosslinking [4]. The polymers used in technique generally have acrylate or methacrylate groups which can be polymerized quickly under the light [8,9]. In the light of this information, in this work, glycidyl methacrylate (GMA), which is the acrylic monomer, was grafted on the chitosan (CTS) backbone and thus chitosan-graft-glycidyl methacrylate (CTS-g-GMA) was produced. Then, CTS-g-GMA and poly(ethylene glycol) diacrylate (PEGDA) was photo-crosslinked under UV light to obtain CTS-based hydrogel.

1.2 Biopolymers for Hydrogel Fabrication

The main components of the hydrogels used in biomedical fields are mostly natural polymers like alginate, collagen, agarose, fibrin, hyaluronic acid (HA), cellulose and CTS. These biopolymers have specific properties according to their sources and chemical structure. HA, fibrin and collagen are obtained from mammalian tissues. Alginate and agarose are marine algal polysaccharides [9,10]. Collagen is an

amphipathic polymer showing good cell-matrix interaction which is used mostly in tissue engineering. It may cause antigenicity in body [11]. Collagen hydrogels can be produced via physical interactions. But, these hydrogels exhibit poor mechanical properties mostly [10]. Chemically crosslinked collagen-based hydrogels were fabricated for improving mechanical properties [12].

HA is used in wound healing and tissue engineering which found in extracellular matrix [13]. Native HA degrade rapidly in living organisms [14]. Its poor mechanical properties can be enhanced by producing HA-based hydrogels. Network structure of the hydrogels protect the HA against the degradation [13,14].

Fibrin is used as a wound healer in surgery which doesn't cause a toxic degradation or inflammatory reactions in the body. Fibrin gels, which have poor mechanical properties, can be show a rapid enzymatic degradation. There are several methods to improve the degradation kinetics and mechanical properties of them like optimizing of the polymerization conditions, combining fibrin gels with other natural (HA) or synthetic (polylactic acid, polycaprolactone) polymers [10,11,13].

Cellulose is the most plentiful biopolymer on Earth which is important component of the plants (Plant cellulose) besides that some species of bacteria such as acetobacter, xylinum can synthesize cellulose, called as bacterial cellulose. Cellulose has a high crystalline structure which makes it insoluble in water and common organic solvent. In preparation of cellulose-based hydrogels, cellulose derivatives (cellulosics) are used to overcome this drawback. Cellulose and cellulosics are biocompatible. But it should be noted that cellulose is a biodurable material because human body has no ability to synthesize cellulases which is the enzyme catalyze the decomposition of cellulose [15,16].

Alginate gels are created easily by means of divalent cations (Ca^{+2}, Mg^{+2}). However, losing of these ions causes uncontrollable and incalculable dissolution. Covalent crosslinking of alginate enhances mechanical and/or swelling properties [10,11].

Agarose forms thermally reversible gels which can dissolve in aqueous media at elevated temperatures (above 65 ^{o}C) and it forms gel again with reducing temperature. Although the agarose hydrogels are stable at body temperature (in the temperature range 17–40 ^{o}C), agarose shows low bioactivity [10,11].

CTS is another natural biopolymer which is prepared by deacetylation of chitin. It is an abundant natural polysaccharide as well as cellulose in the world. Approximately 10^{10} tons of chitin is obtained from cell walls of fungi, the exoskeletons of arthropods, insects and beaks and internal shells of cephalopods and mollusks. It consists of glucosamine and acetyl-glucosamine units and numbers of these units are related with the deacetylation degree of the chitin [17,18].

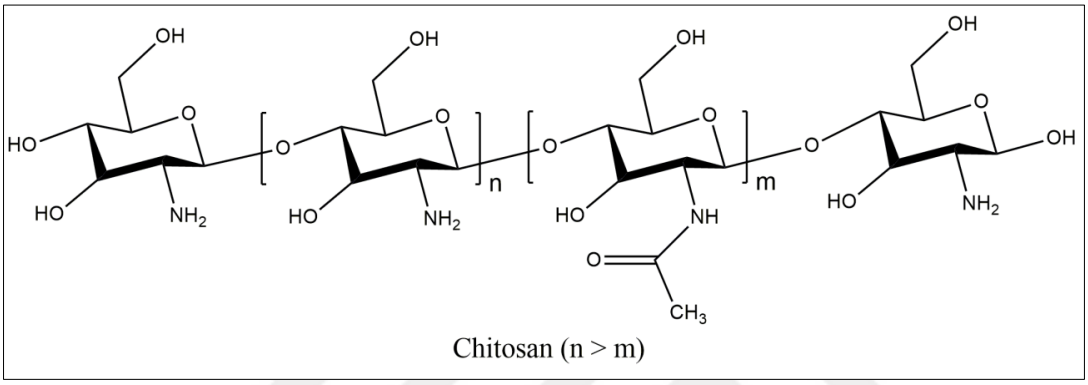

Figure 1.4 Chemical structure of the CTS

CTS is chosen as main component for the produced hydrogels in this study due to the unique properties. It has low toxicity and good biocompatibility like aforementioned other biocompatible natural polymers. When CTS contacts with the human body, it shows excellent properties such as bioactivity, antimicrobial activity, and enzymatically biodegradability. Owing these properties, it is used in biotechnology field such as drug delivery systems [19] and biosensor applications [20]. Although this biopolymer has many advantages including, nontoxicity, biodegradability, and biocompatibility good film-forming ability, pH sensitivity, it has insufficient mechanical resistance limiting the applications. In order to improve the thermal and mechanical properties, CTS which has amino and hydroxyl chemical functional groups is modified by various methods. The grafting of acrylic monomers onto the CTS backbone is one of modification methods [17,18].

1.3 Electroconductive Hydrogels

Electroconductive hydrogels (ECHs) are multifunctional smart materials that, incorporates the property of electrical conductivity and water retention [21]. These versatile materials can be extensively classified based on preparation methods into two groups [22]. In one of these method, the property of electrical conductivity is improved by the addition of conductive particles such as carbon nanotubes [23], graphene-family materials (graphene, graphene oxide (GO), reduced graphene oxide (RGO) etc.) [24–26], metallic nanoparticles [27], into the hydrogel structure. Another method is the modifications of hydrogels with inherently conducting polymers (CPs) including polyaniline (PANI) [21], poly(pyrrole) [15], Poly(3,4-ethylenedioxythiophene) (PEDOT) [28].

Conducting polymers are attractive materials for researchers but some disadvantages limit their applications, especially biomedical applications. For instance, in some cases toxicity (depends on polymer type, polymerization method and purification) and non-biodegradability of conducting polymers are limitations. Polymeric network of a hydrogel can cover the conducting polymer and prevent the release of it to body. In addition, formed ECH reflects its electrical conductivity [29]. Film and coating applications may become impossible with conducting polymers. Preparing ECHs with conductive polymers overcome this drawback [30]. Biocompatibility is very important for electrodes used in biomedical devices. Surface modifications of metal electrodes with biomolecules enhance the biocompatibility. Using ECHs in bioelectrode fabrication can be very useful especially for in-vivo applications due to similar properties of hydrogels such as high water content, rubbery and soft state to tissues [31].

1.3.1 Advantages of RGO for Synthesis of ECH

Recently, graphene-family materials are attractive for researchers in ECH hydrogel fabrication due to beneficial properties. The sp^2-hybridized carbon atoms provide the conductivity to these molecules [32]. Graphite which is found in nature abundantly has 3-D and layered chemical structure. Van der Waals forces build up 3-D chemical structure of graphite by keeping together layers [33]. Chemical inertness of the graphite is a disadvantage for applications [34]. Graphene is a two-dimensional (2-D) and mono

or few layered form of graphite which is very attractive cause of superior features like biocompatibility, large surface area, high thermal conductivity and excellent mechanical flexibility [35,36]. In addition, graphene exhibits marvelous electrical properties including high electron mobility and electrical conductivity. It is explained by the band structure of the graphene. If the energy of the electrons is shown in function of their momentums the energy bands turn into parabolas for metals and insulators. Graphene exhibits an unusual behavior, the energy bands form two circular cones called as Dirac cones which connected one with the other at their extremities (Figure 1.5). So, the electrons of graphene behave as if they have no mass and can travel long distances without scattering along the plane structure with same velocity and absolutely no inertia. [37].

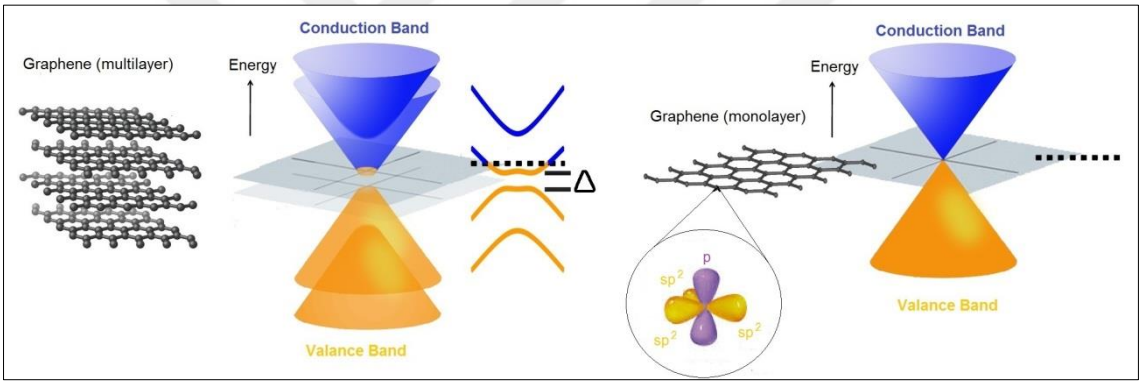

Figure 1.5 Conic energy bands of graphene

Unfortunately, easy aggregation and poor dispersion in aqueous media due to the native hydrophobicity of graphene restrict its processing [35]. These are disadvantages for generating a homogenous conductive system in hydrogel network. To overcome these obstacles, GO obtained from graphite and RGO obtained from reduction of GO which are most widespread derivatives of graphene [36]. GO contains plenty of oxygen atoms in functional groups (hydroxyl, epoxide and carboxyl groups) covalently bonded to sp^3-hybridized carbon atoms. Hydrophilic GO demonstrates a good dispersion in various polar organic solvents and water [38]. The sp^3-hybridized carbon atoms eliminate the honeycomb lattices structure consisting of sp^2-hybridized carbon atoms and this causes a loss of conductivity [39]. So, RGO is obtained by reduction of GO to improve conductivity and restore the sp^2-hybridized carbon system. By this way, a conductive

molecule, which is capable of forming interactions to obtain composite materials with functional pendant groups, can be obtained. In addition, dispersion in many organic solvent and water, easy synthesis and mechanical flexibility properties make RGO an advantageous material for ECH applications [36,40].

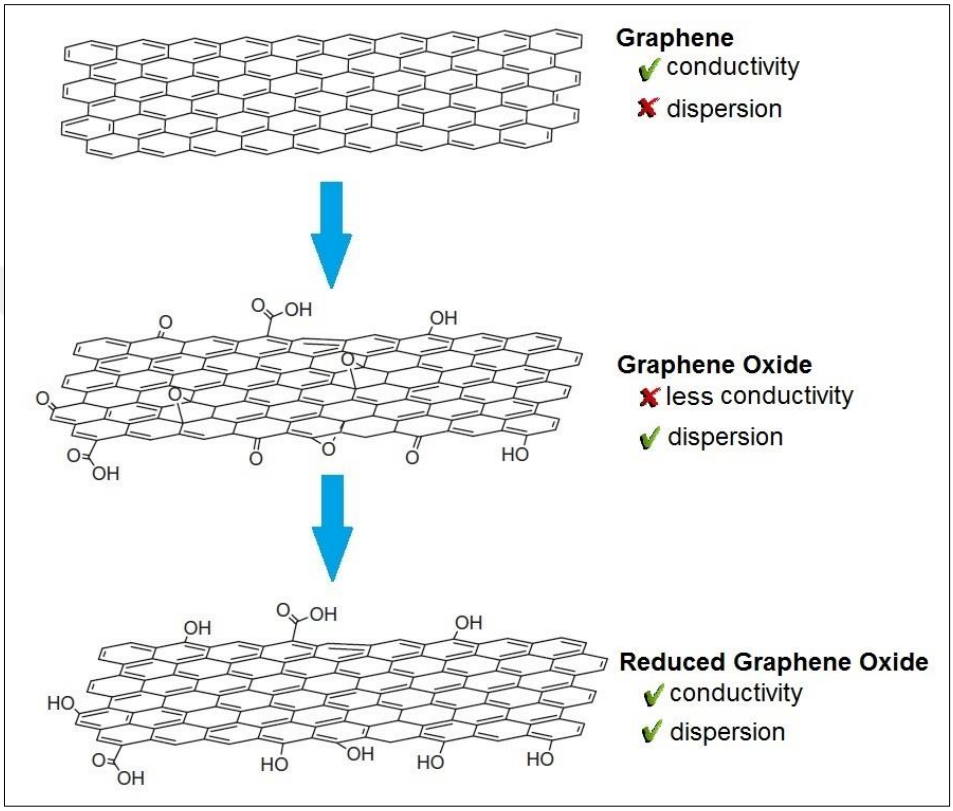

Figure 1.6 Chemical structures of graphene, GO and RGO

Cytotoxicity of the graphene-family materials depends on concentration in samples, cell type, synthesis methods and functionalization [37].

1.3.2 Advantages of PANI for Synthesis of ECH

Fabricating an ECH with inherently conducting polymers is a common and effective approach [21,22,41]. Conductive electroactive polymers such as polyaniline, polypyrrole and PEDOT can conduct charge like metals and are also flexible like conventional polymers. CPs are used in many applications such as; optical devices, polymeric light emitting diodes (LEDs), electrochromic windows and displays,

chemical and biological sensors, corrosion protective coatings, electrodes of batteries and electromagnetic shielding materials [42,43]. Some common CPs are listed in Table 1.1.

Table 1.1 List of some important CPs and repeating units

Conducting Polymer	Repeating Unit
Polyacetylene (PA)	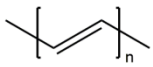
Polythiophene (PTs)	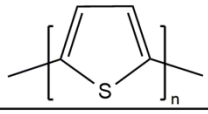
Polyparaphenylene (PPP)	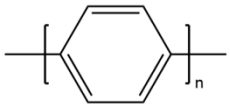
Poly(3,4-ethylenedioxythiophene) (PEDOT)	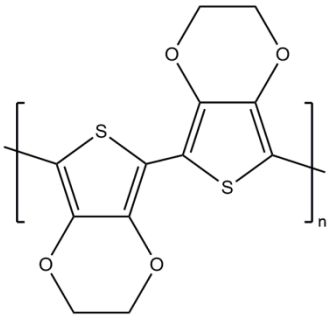
Polypyrrole (PPy)	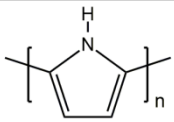
Polyaniline (PANI)	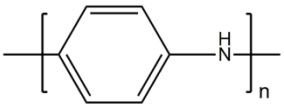

PANI is the one of the most used conducting polymer because of the good environmental stability, high electrical conductivity, easy and low cost synthesis [21], [22]. Polyconjugated planar system of PANI, which consists of sequential series of phenyl rings and nitrogen containing groups, provides a charge transfer path for π electrons in phenyl rings and the electron pair of nitrogen located along the plane. PANI can be found in one of three forms according to oxidation states [44].

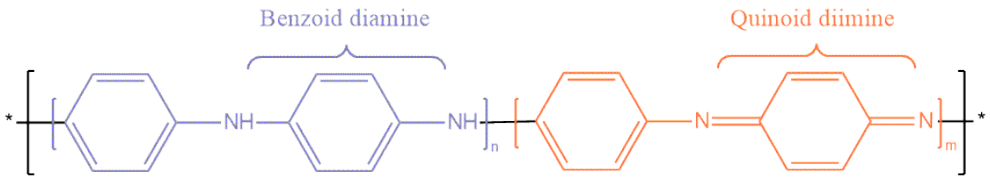

Figure 1.7 Chemical structure of PANI

Pernigraniline form is the fully oxidized state of the PANI (n=0 in Figure 1.7), conversely leucoemeraldine form is the fully reduced state (m = 0 in Figure 1.7). The half oxidized emeraldine form of PANI (n=m in Figure 1.7) is the most advantageous form due to the high stability and conductivity. [43,45]. Both leucoemeraldine and pernigraniline forms of PANI turn into emeraldine form simultaneously if there is no external potential [44].

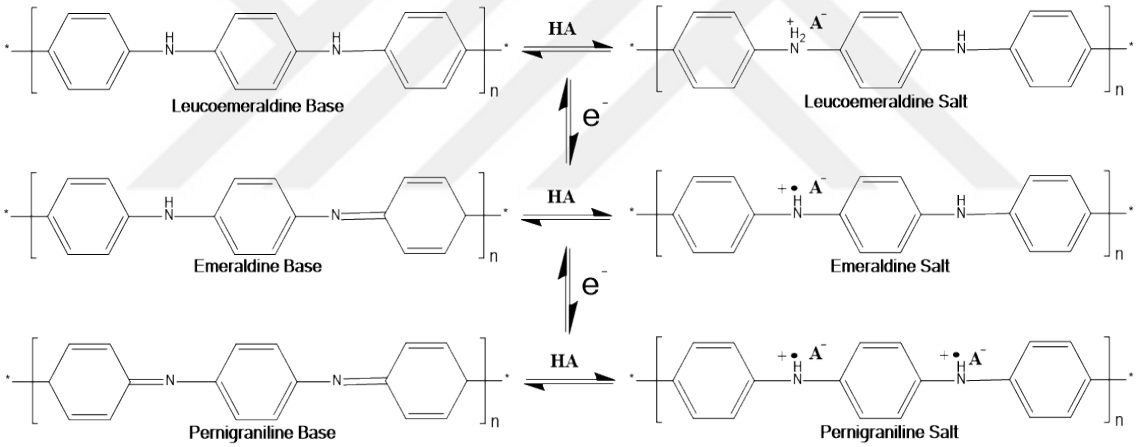

Figure 1.8 Polyaniline forms

Polyaniline is doped with strong acids. Positive polarons occur during oxidation of PANI and is stabilized by the acid anion and proton. This increases the mobility of delocalized valance electrons. So, conductivity of the doped emeraldine form of the PANI is higher very much than that of other forms [41,44,45].

Petr Humpolicek et al published a detailed study about the biocompatibility of polyaniline. According to the study, although PANI does not cause skin irritation and sensitization, it shows cytotoxicity. However, the cytotoxicity was decreased

remarkably by a purification step subsequent to polymer synthesis. Because, the main reasons of cytotoxicity are by-products and residues of synthesis reaction [46]. Besides that, non-biodegradability limits the usage of PANI in some biomedical applications [22,43]. PANI can be modified to overcome these obstacles and enhance the biocompatibility [22].

1.3.3 ECHs in Biomedical Applications

Hydrogels are similar to living tissues owing to high water content, soft and rubbery state so they are preferred mostly in biomedical fields [8]. As mentioned before, ECHs are formed by combination of hydrogels and conductive materials such as conductive polymers, graphene-family materials. ECHs are versatile materials and mostly used also in biomedical fields such as tissue engineering [47], biosensors [48].

Undoubtedly, biocompatibility is extremely important for biomedical applications (especially in vivo applications). If a foreign object enters the body, physicochemical reactions will be started to respond it. ECHs can be fabricated as biocompatible and implantable materials. For instance, PC12 cells exhibited better growth and proliferation on Poly(2-hydroxyethyl methacrylate)-polypyrrole (pHEMA-Ppy) hydrogels than bare hydrogel or PPy (Figure 1.9). Coating of an in vivo biomaterial with an ECH membrane makes a positive impact on the material with respect to non-electroconductive hydrogel membrane [42,49]. Another example, G. Justin and A. Guiseppi-Elie produced non-ECHs, ECHs and electropolymerized PPy for coating on microdisc electrode arrays (MDEAs). Coating applications to MDEA transducer devices showed that ECH film coatings exhibits higher peak currents accompanied the ferrocene monocarboxylic acid with respect to other applications in cyclic voltammetry voltammograms. The results demonstrated that ECHs are very promising coating materials for implantable biosensors to enhance sensitivity, redox signal and limits of detection [48].

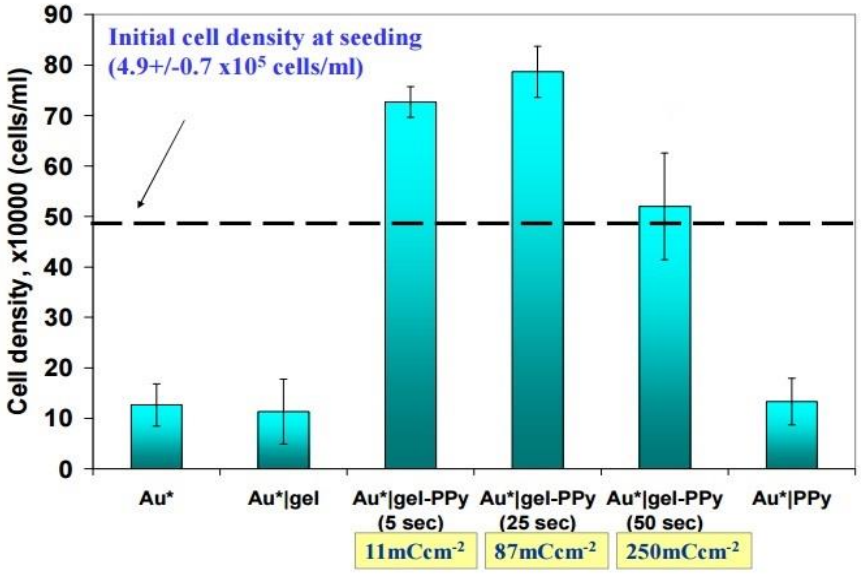

Figure 1.9 PC12 cell densities after 4 days incubation on Au*, Au*|hydrogel, Au*|PPy, Au*|hydrogel-PPy (electropolymerization times: 5, 25 and 50 s) [42]

Biosensors provide value medical information about patient's status. So, these devices are important components of healthcare. ECHs are unique materials for biosensor fabrication and researchers have been studied related to this subject. Christian Kotanen and A. Guiseppi-Elie synthesized bioactive electroconductive and non-electroconductive hydrogels which were used as hosting membranes for lactate oxidase enzyme and coated electrodes. As seen from Table 1.2, the bioactive electroconductive hydrogel membrane exhibits highest sensitivity and lowest detection limit [50].

Christian N.Kotanen and others coated platinum electrodes with glucose oxidase enzyme loaded PPy-hydrogel composite to fabrication of an amperometric biosensor for glucose detection. As a result, the study was found suitable for biosensors, bionics and bioelectronics applications [51].

Table 1.2 Bioanalytical performance of lactate biotransducers produced from planar metal electrodes, microdisc electrode arrays, non-electroconductive hydrogels and electroconductive hydrogels. p(HEMA) = poly(hydroxyethyl methacrylate), PEGLOx = PEGylated lactate oxidase and PPy = poly(pyrrole-co-4(3-pyrrolyl)butyric acid) [50]

Electrode Type	Membrane Type	Linear range (mM)	Sensitivity (uA mM^{-1})	Detection Limit (mM)
PME-Au	P(HEMA)-PEGLOx	0.1 – 3.0	0.0662	0.0900
MDEA50-Au	P(HEMA)-PEGLOx	1.0 – 90.0	0.0033	0.8000
MDEA50-Au	P(HEMA)-PPy-PEGLOx	0.002 – 0.5	1.4122	0.0018

2 MATERIAL AND METHOD

2.1 Materials

Acetic acid (CH_3COOH), potassium hydroxide (KOH), potassium nitrate (KNO_3), ethanol (EtOH), acetonitrile (C_2H_3N), tetrahydrofuran (THF), ammonium peroxodisulfate (APS), aniline ($C_6H_5NH_2$), hydrochloric acid (HCl), hydrogen peroxide (H_2O_2) (30% by weight) and sulfuric acid (H_2SO_4) (98% by weight) were obtained from Merck and used without any purification. Hydrazine solution (35 wt. % in water) Hydroquinone, CTS, GMA, PEGDA, Graphite (powder <20 μm, synthetic) and 2-Hydroxy-4′-(2-hydroxyethoxy)-2-methylpropiophenone (photoinitiator) were purchased from Sigma Aldrich. (4-[3-(4-iodophenyl)-2-(4-nitrophenyl)-2H-5-tetrazolio] 1,3benzenedisulfonate) (WST-1) cell proliferationreagent was obtained from Roche. Dulbecco's Modified Eagle Medium was provided from PAN Biotech.

2.2 Synthesis of (CTS-g-GMA)-PEGDA Hydrogel

Firstly, CTS-g-GMA was synthesized in weight ratio CTS:GMA of 2:1. A known amount of CTS (approximately 1 gram) was dissolved in 0.4 M acetic acid with magnetic stirring. A small amount of hydroquinone was added to the solution to prevent the formation of poly(glycidyl methacrylate) (PGMA). The flask which contains the mixture was placed into an ice bath. The prepared mixture in volume ratio GMA:EtOH of 1:3 were slowly added into the flask. Then, pH of the reaction mixture was done 3.8 with addition of 0.5 M KOH. It was heated to 60 °C, nitrogen gas flowed through the flask with constant magnetic stirring during 2 hours. The sealed flask was placed into an ice bath to end the reaction.

40 ml of acetonitrile was poured in a flask which was placed in a magnetic stirrer. The reaction mixture was dribbled slowly into the acetonitrile to precipitate the product. When the acetonitrile was observed blurry, this process was stopped. During the reaction, PGMA may form by self-polymerization; the product was washed with THF to remove this polymer. White solid products were placed vacuum oven for 72 hours at room temperature for drying.

After the drying, (CTS-g-GMA)-PEGDA hydrogels were synthesized with different concentrations of grafted polymer and weight ratios of (CTS-g-GMA)/PEGDA. PEGDA was used as a crosslinker. To determine optimum conditions, swelling test was performed with the obtained hydrogels having different component ratios. According to the test results, the chemical synthesis procedure was conducted as follows:

CTS-g-GMA (250 mg dry weigh) was placed in a dark bottle then 10 mL distilled water was added. CTS-g-GMA was dissolved in distilled water until obtain a homogeneous solution, then 450 µL PEGDA was added. The dark bottle was placed in the magnetic stirrer. After 10 minutes, 50 mg of photoinitiator (2-Hydroxy-4′-(2-hydroxyethoxy)-2-methylpropiophenone) (Figure 2.1) was added.

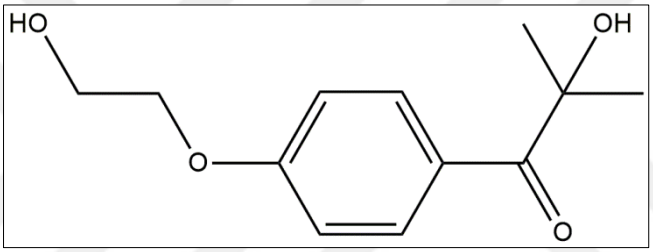

Figure 2.1 Molecular structure of the photoinitiatior

The mixture was stirred for 10 minutes at 45 °C, and then stirring was continued for 1 hour at room temperature to ensure complete dissolution of the photoinitiator. 950 µL of the homogeneous mixture was injected into custom-made, round, glass molds by a micropipette. They were placed into the photoreactor (Kerman Photoreactor) and exposed to 365 nm UV light at room temperature for 5, 10, 15, 20 minutes.

2.3 Synthesis of ECHs

In this study, two different approaches were applied to fabricate conductive hydrogels. According to first approach, RGO was encapsulated into the (CTS-g-GMA)-PEGDA hydrogel during the photo-crosslinking process. In the second approach, PANI was absorbed by the preformed (CTS-g-GMA)-PEGDA. Both of fabrication processes were given below in detail.

2.3.1 Synthesis of RGO-based Conductive Hydrogel

2.3.1.1 Synthesis of Reduced Graphene Oxide (RGO)

GO was obtained by using a modified Hummers method from graphite powder [40,52,53]. In a typical procedure, 1 g graphite and 0.5 g KNO_3 was slowly added respectively into the stirred concentrated 23.3 mL of H_2SO_4 (98%) that was kept in an ice bath. After about 15 min stirring, 3 g of $KMnO_4$ was added little by little into the mixture with continuous stirring. Then, a sand bath was prepared at 35 °C. The mixture that was in a beaker was placed into the sand bath and kept magnetic stirring for 30 minutes. Subsequently, 50 mL of distilled water was poured into the beaker. After the addition of water, the mixture was stirred at 90 °C for 15 minutes. 167 mL of distilled water was added and kept stirring for 10 minutes. 5 mL of 30% H_2O_2 was added gingerly.

The warm solution was transferred to conical Eppendorf tubes; centrifugation was carried out at 6500 rpm for 10 minutes. The product was filtered and washed with 10% by volume HCl. This centrifugation and washing processes was repeated (3-4 times) until the particles were disappeared in the liquid fraction. Finally, the tubes were placed in an oven at 65 °C for 48 hours. Subsequently, the obtained graphite oxide was dispersed in 200 mL distilled water by ultrasonication to form a colloidal graphene oxide suspension. For reduction of GO, 2 mL of hydrazine (35 wt. %) was slowly added and the mixture was kept stirring for 24 hours at 100 °C. It was cooled to room temperature and filtered by a vacuum flask and a Buchner funnel. After washing with 100 mL of methanol and 100 mL of distilled water, the filtrate was dried in vacuum oven at room temperature.

2.3.1.2 Synthesis of the RGO-Based Hydrogels

RGO-containing hydrogels were fabricated in four different weight ratios of RGO (0%, 3%, 5%, 10%, and 15%). Calculated amounts of RGO and 1 mL of EtOH put inside the sealed tubes which were placed into the ultrasonic bath for 15 min. CTS-GMA-PEGDA polymer solution prepared by procedure explained in section 2.2 was added to the RGO suspension. They were stirred with a thin rod and placed into the ultrasonic bath for 30 min. again. 1 mL of each mixture was injected into custom-made, round, glass molds by

a Pasteur pipette. The glass molds were placed in the photoreactor. The hydrogel RGO-free one was exposed UV light for 15 min. The hydrogels including RGO did not polymerize completely for the same UV time. Therefore, they were placed in photoreactor further 5 min. more.

2.3.2 Synthesis of PANI-based Hydrogels

(CTS-g-GMA)-PEGDA hydrogels were fabricated by photo-crosslinking technique for 15 minutes UV exposure times (The procedure explained in section 2.2 in detail). The obtained hydrogels were immersed into the three different concentration aniline solutions, 0.08 M, 0.16 M, and 0.32 M, prepared in 1 M HCl for 12 hours, separately. Equimolar amount of APS as an initiator to aniline was added to the mixtures. After three hours, hydrogels were taken for washing. The white color hydrogels became dark green–blue color because of the polymerization of the aniline in the hydrogel matrix. Washing process was performed in 250 mL of distilled water by mechanic stirring for four days. It is worthwhile to mention that not only aniline convert into the polyaniline in the hydrogel matrix but also polyaniline which form in the reaction medium diffuse into the hydrogel network. The quite hydrophilic character of the obtained CTS-based hydrogel is responsible for both mechanisms stated above. After washing, hydrogels were dried at room temperature in petri dishes for 24 hours.

2.4 Characterization of Hydrogels

2.4.1 Fourier Transform Infrared (FTIR) Spectroscopy Analysis

The molecular structure of hydrogels, graft polymer and CTS were verified by a FTIR spectroscopy. FTIR analysis was carried out with a Perkin Elmer Spectrum One FTIR with attenuated total reflectance (ATR) unit and the membranes were scanned in the range of 600 and 4000 cm^{-1} with 4 cm^{-1} resolution averaging 120 scans.

2.4.2 X-Ray Diffraction (XRD) Spectroscopy Analysis

The crystallinity of hydrogels were tested using XRD spectroscopy (Bruker D2 Phaser X-ray diffractometer using Cu Kα irradiation λ=1.54184 °A) at the speed of 5°/min and in the range of 0-60°. Working current is 10 mA and voltage is 30 kV.

2.5 Thermal Behavior of Hydrogels

The thermal stability of the hydrogels, graft polymer and CTS was determined by thermogravimetric analysis (TGA) and differential thermal analysis (DTA). To obtain weight loss profile and DTA curves of the CTS, graft polymer and hydrogels, thermal analyses were conducted performing Seiko EXSTAR 6000-TGA/DTA 6300 model instrument with a heating rate of 10 °C min^{-1} under a nitrogen atmosphere

2.6 Cytotoxicity Test

Cytotoxicity of conductive hydrogels was explored by means of Murine Fibroblast L929 cell line and WST-1 cell proliferation and viability test. L929 bioassay system at 70% confluence from exponential-phase culture and was washed with phosphate-buffered saline. It was separated with 0.1% trypsin-EDTA. After that, sterilized hydrogel samples were putted into 24-well cell culture plates. 1 mL of cell-DMEM solution (5×10^4 viable cells/mL) was seeded onto the hydrogels and incubated at 37 ^oC for 24 h under 5% CO_2 medium in a humidified incubator. 5×10^4 viable cells in 1 mL cell-DMEM complete medium were seeded into free control wells. After 24 h, 1000 μL of WST-1 solution was added to each well and incubation was carried out for 2 h. Then, absorbance value of WST-1 for each sample was determined by means of a Promega GloMax-Multi+ detection system at 450 nm.

2.7 Swelling Properties of Hydrogels

A simple gravimetric method was employed for the swelling test. It was based on measuring the equilibrium water content in the hydrogels after immersing it in distilled water for a certain period at a fixed temperature. The weighed dry hydrogel samples were placed in sealed tubes with 10 mL of distilled water for 24 hours and the tubes were placed in an orbital shaker-incubator at 37 ^oC. Following, the swollen hydrogels were weighed. Swelling ratios were calculated according to this formula [41],

$$\text{Swelling Ratio } \% = \frac{W_s - W_d}{W_d} x100 \quad (2.1)$$

Ws: Swollen mass of hydrogel, mg

Wd: Dry mass of hydrogel, mg

2.8 Electrical Conductivity of ECHs

The electrical conductivity of the hydrogels was derived from the sheet resistivity determined by the four-point probe technique which is a characterization tool used widely for examining the electrical properties of solids and thin films [54]. A four-point probe system has a probe head consists of four thin and small metallic probes which made contact with the sample surface. In this study Lucas Labs S-302 Four Point Resistivity Probing Equipment which was connected to a Gamry Instruments power source to supply the constant current and to read the voltage, was used.

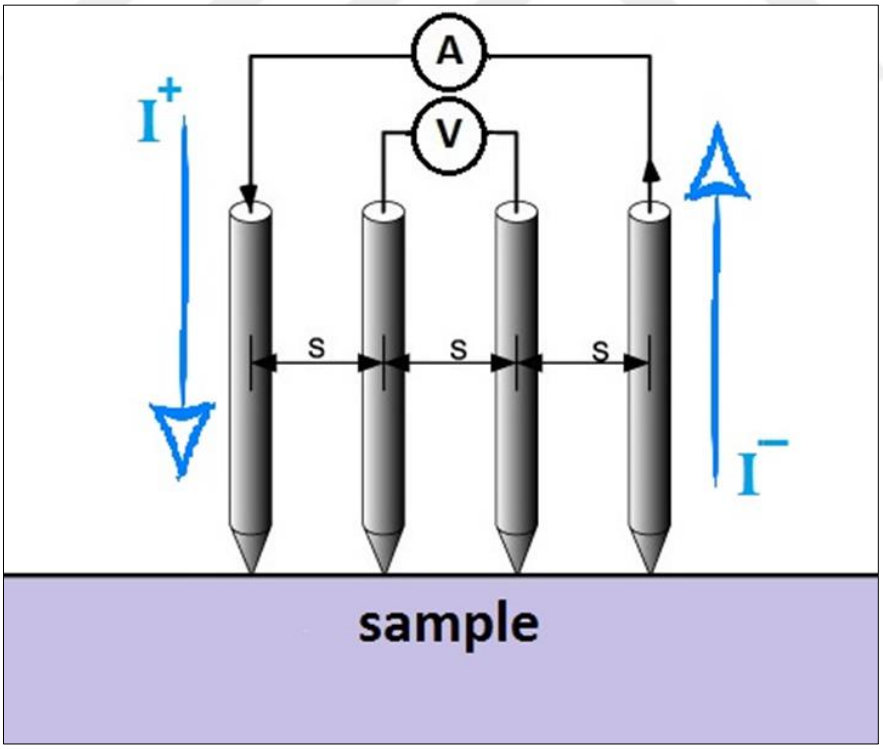

Figure 2.2 Schematic shown of an in-line four-point probe configuration

A current is applied which pass across two outer probes and the voltage is determined through the other inner probes. Thus, the calculation of sheet resistivity ρ according to following equation;

$$\rho = 2\pi s \frac{V}{I} \tag{2.2}$$

where s is the probe spacing, V is the potential difference between the two inner probes, I is the current through the outer pair of probes. Then the conductivity σ is calculated using Equation 2.3 [55].

$$\sigma = \frac{1}{\rho} \tag{2.3}$$

3 RESULTS AND DISCUSSION

In this study, both two approaches were conducted with (CTS-g-GMA)-PEGDA hydrogel. For the first approach RGO containing reactive pendant groups (OH and COOH) was encapsulated into the hydrogel since RGO has advantages such as a low cost of preparation, two dimensional plane structure, large surface area, mechanical flexibility and the dispersion ability in many organic solvents and water [40]. RGO-based materials can be used frequently in various studies such as smart hydrogel production [34], chemical sensors [56], membrane technology [57], catalysts [58], lithium ion [59] and lithium sulfur [60] batteries. In addition, varied biomolecules can be immobilized on RGO owing to non-covalent interactions (hydrogen bonding and π electron interactions) [61]. These unique properties make RGO a convenient component for biosensor applications.

Our second approach for producing an ECH hydrogel is absorption and polymerization of PANI into the preformed hydrogel network. PANI is an appropriate inherently conductive polymer for this study due to the remarkable properties such as easy and low cost synthesis, high and controllable conductivity, and environmental stability [21], [62]. Rechargeable battery systems [63], supercapacitors [64], chemical sensors [65] and biosensors [66] are some potential application areas of PANI.

3.1 Synthesis of (CTS-g-GMA)-PEGDA Hydrogels

The hydrogels were fabricated in two steps. First, GMA was grafted onto CTS backbone to form a hybrid natural-synthetic biopolymer. The reaction mechanism is depicted in Figure 3.1

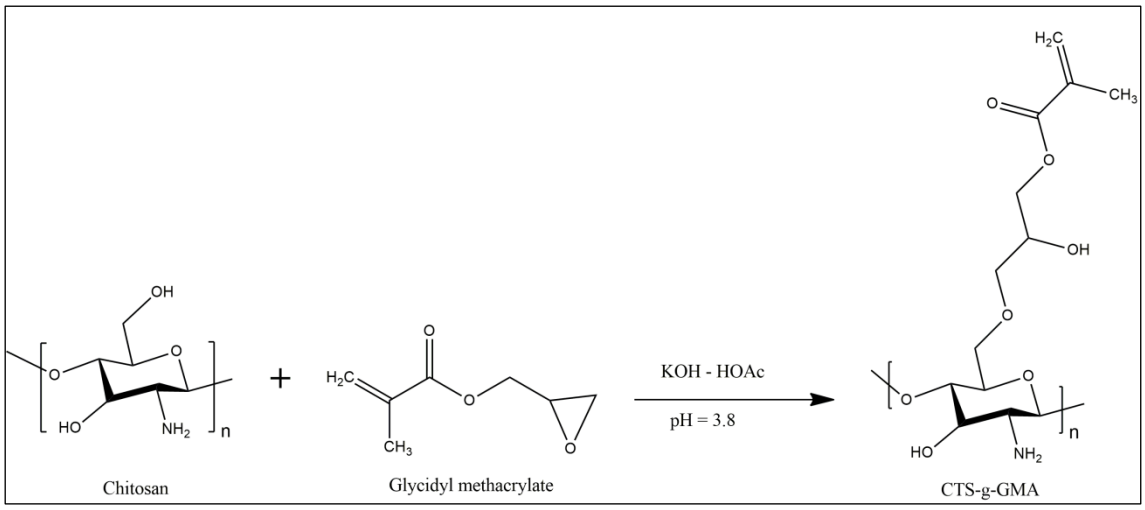

Figure 3.1 Reaction mechanism of synthesis of CTS-g-GMA

In the second step, CTS-g-GMA and PEGDA were photo-crosslinked by using UV irradiation at 360 nm (Figure 3.2)

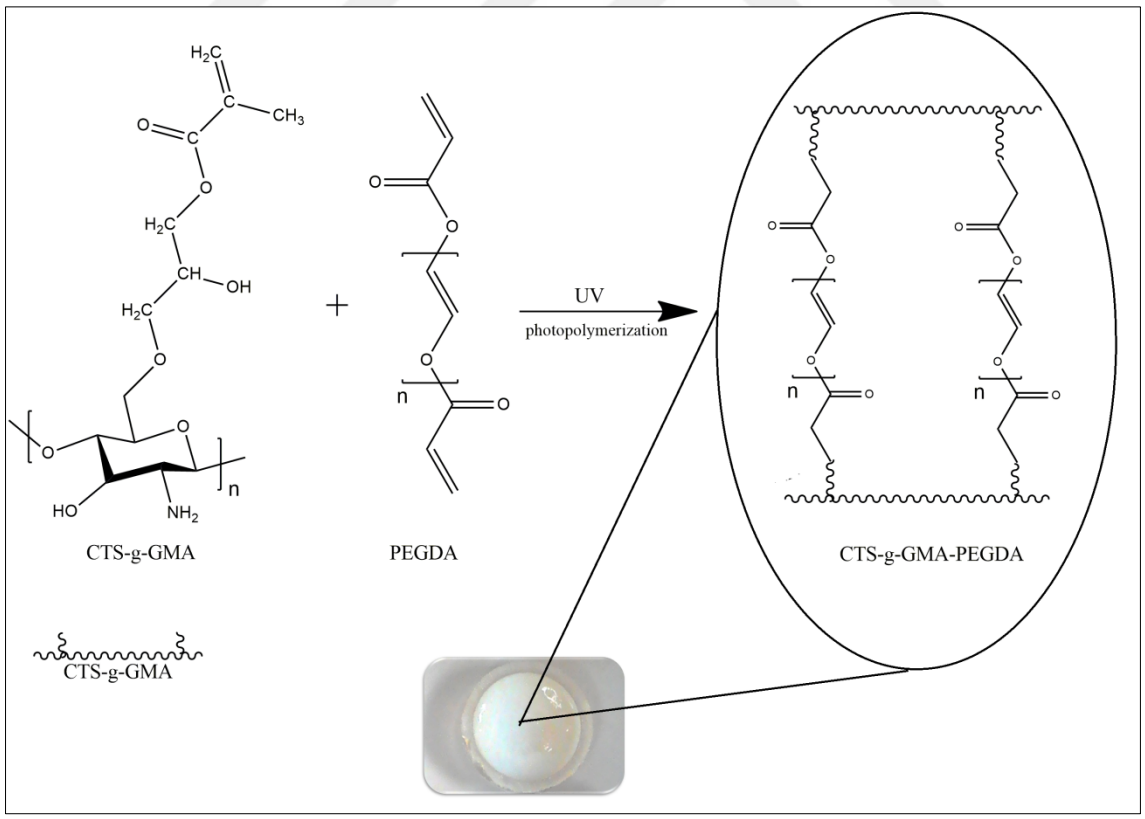

Figure 3.2 Schematic shown of the synthesis procedure of the (CTS-g-GMA)-PEGDA hydrogel

3.1.1 Characterization of [(CTS-g-GMA)-PEGDA] Hydrogel

3.1.1.1 FTIR Spectroscopy Analysis

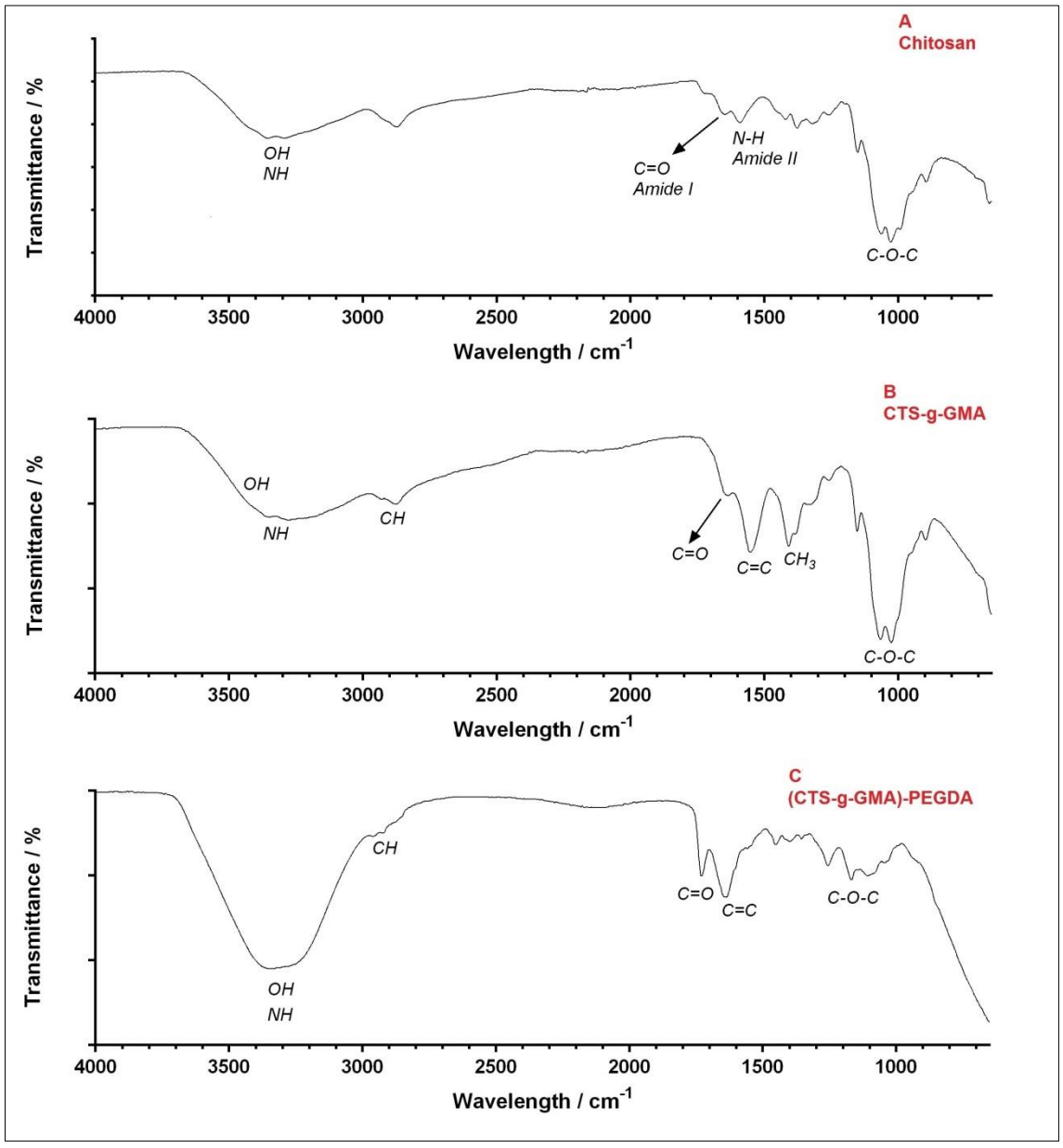

Figure 3.3 FTIR spectrums of (A) CTS (B) CTS-g-GMA (C) (CTS-g-GMA)-PEGDA

Figure 3.3 shows FTIR spectrums of CTS, CTS-g-GMA and (CTS-g-GMA)-PEGDA. Wide bands at 3300 cm^{-1} in all spectrums represent the stretching vibrations of O-H and N-H bonds. The peaks located at 1660 and 1600 cm^{-1} are associated with C=O stretching (Amide I) and N-H bending (Amide II) vibrations of amide groups in CTS,

respectively. These two peaks (Amide I and Amide II) demonstrate that CTS is partially deacetylated. The intense peak appearing at 1050 cm^{-1} is due to stretching vibrations of ether functionality of CTS.

In comparison with the FTIR spectrum of CTS, CTS-g-GMA displayed C=C stretching absorption peak at 1550 cm^{-1} and pendant C-H stretching absorption peak at 1405 cm^{-1}. Furthermore, the carbonyl peak observed at 1660 cm^{-1} was shifted to 1640 cm^{-1} in CTS-g-GMA spectrum as a result of grafting procedure. The observed results pointed out that GMA was successfully grafted onto the CTS backbone.

The intensities of stretching vibrations of -OH and C=O groups increased significantly in the spectrum of (CTS-g-GMA)-PEGDA due to the increment of these groups in the hydrogel structure with addition of PEGDA.

3.1.2 Thermal Behavior of (CTS-g-GMA)-PEGDA Hydrogel

As seen in TGA and DTG curves, CTS (Figure 3.4 A and B) showed two significant drops in mass at around 68.00 °C and 308.50 °C. While the first weight-loss (from 25.40 to 143.2 °C) can be assigned to the elimination of water, the second weight-loss is due to the decomposition of cyclic moiety.

As seen from Figure C-D, CTS-g-GMA has a three well-defined weight loss region at 61.8 °C, 145 °C, and 277 °C. These regions are related with the water evaporation, GMA loss, and main degradation of grafted polymeric structure (CTS), respectively. It can be noted that CTS-g-GMA has lower thermal degradation temperature (277 °C) compared to CTS (308.50 °C) [67,68].

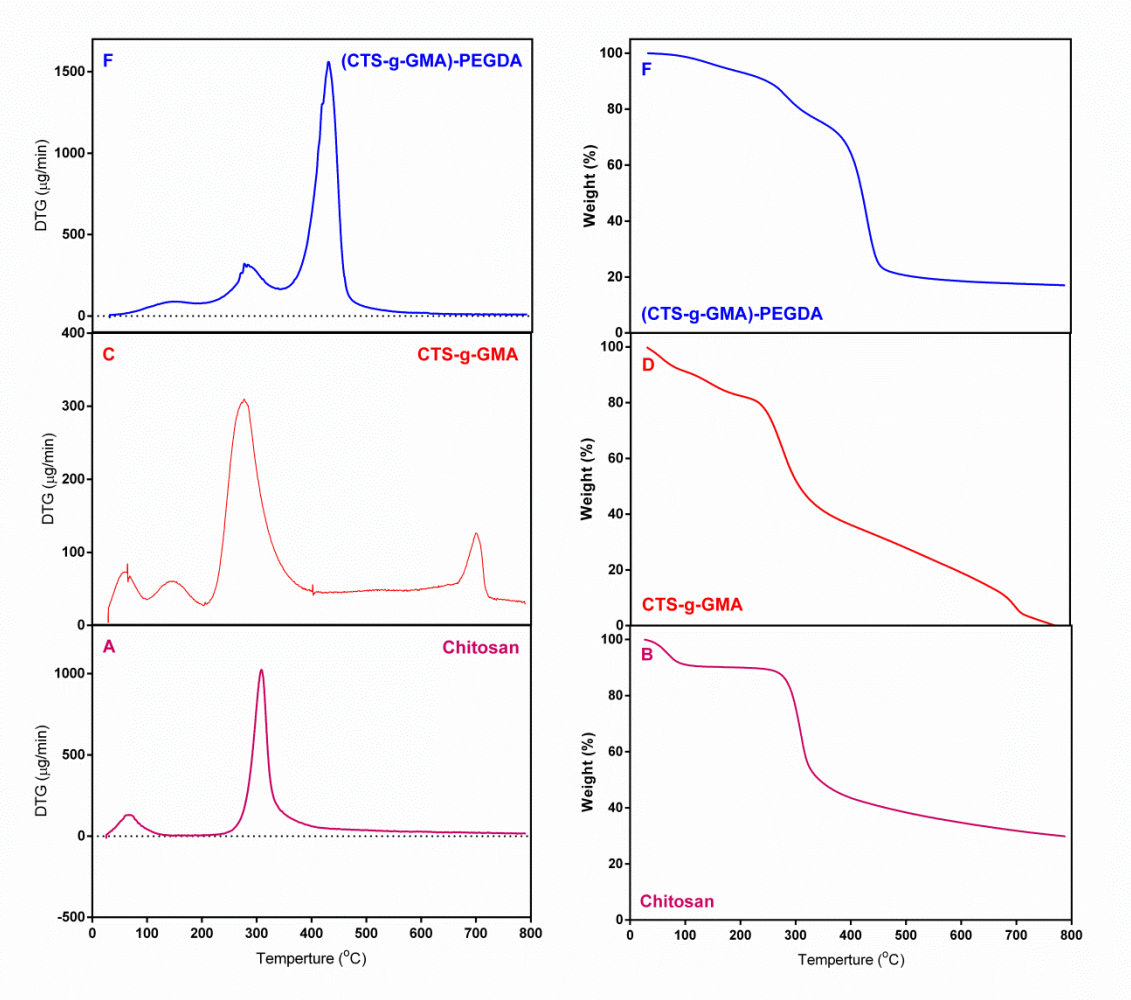

Figure 3.4 DTG and TGA curves of (A and B) CTS, (C and D) CTS-g-GMA and (E and F) (CTS-g-GMA)-PEGDA

Three weight-loss steps were also observed for (CTS-g-GMA)-PEGDA. The first one between 62.7 °C and 194.66 °C is due to bounded water in the structure of hydrogel, the second weight-loss between 201.69 °C and 339.82 °C corresponds to chitosan decomposition. The last weight-loss which appears between 345.90 °C and 553.23 °C is related with the main decomposition of the crosslinked hydrogel.

From the results, it can be stated that thermal decomposition temperature of (CTS-g-GMA)-PEGDA (427 °C) is much higher than that of CTS-g-GMA (277 °C) and chitosan (308.50 °C) since the structure of (CTS-g-GMA)-PEGDA is chemically crosslinked network, which provides thermal stability to hydrogel.

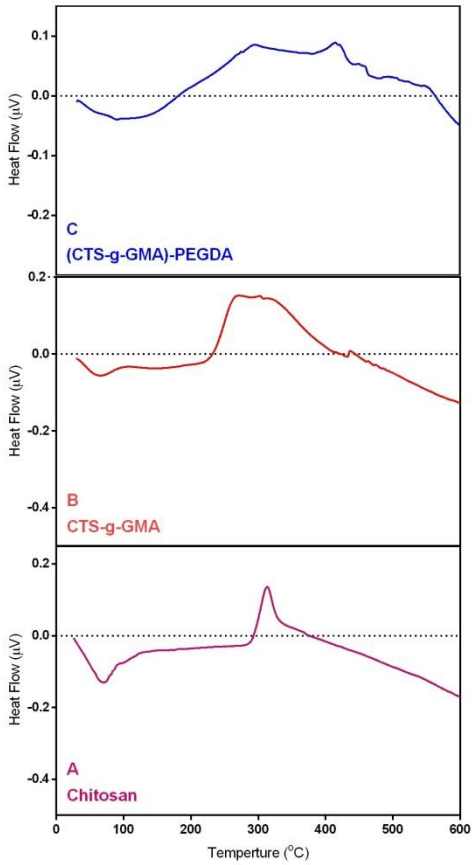

Figure 3.5 DTA curves of (A) CTS (B) CTS-g-GMA (C) (CTS-g-GMA)-PEGDA

In the DTA spectrum of CTS there are one endothermic peak at 68.3 ^{o}C and one exothermic peak at 313 ^{o}C which is due to thermal decomposition of saccharide ring of chitosan. DTA curve of the CTS-g-GMA exhibited two endothermic peaks and one wide exothermic peak at 64.9 ^{o}C, 151 ^{o}C and 288 ^{o}C, respectively which are proved three weight-losses in TGA curve. In case of (CTS-g-GMA)-PEGDA, one endothermic peak and two exothermic peaks were observed at 93.2 ^{o}C, 296 ^{o}C and 415 ^{o}C, respectively. The endotherm can be related with evaporation of bounded water molecules into the hydrogel network. The exothermic peaks can be assigned to partial and main decompositions of the crosslinked hydrogel.

3.1.3 Swelling Properties of (CTS-g-GMA)-PEGDA Hydrogel

To investigate the swelling behaviors of the (CTS-g-GMA)-PEGDA hydrogels prepared with different polymer concentrations 1% - 1.5% - 2.5% - 5% - 7.5%. The samples that

prepared in 1%, 1.5%, 2.5%, 5% concentrations dissolved in distilled water in the course of the swelling test. Then, for 7.5% concentration, (CTS-g-GMA)-PEGDA hydrogels were synthesized in weight ratios (CTS-g-GMA):PEGDA of 1:1 and 1:2. While, hydrogels including the weight ratio of (CTS-g-GMA):PEGDA of 1:1 were divided two or three pieces in distilled water, hydrogels having that of 1:2 were swollen in distilled water by protecting their integrity. It should be noted that the crosslink density of the hydrogels increased with increasing the amount PEGDA which is used as a crosslinker into the hydrogel matrix.

The polymer solutions were exposed to the UV light at room temperature for, 5, 10, 15, 20 minutes and all conditions kept constant to examine effect of UV time on hydrogel swelling behavior. The obtained hydrogels were weighed at dry and wet state. Swelling ratios of them were calculated and showed in Figure 3.5 with UV times.

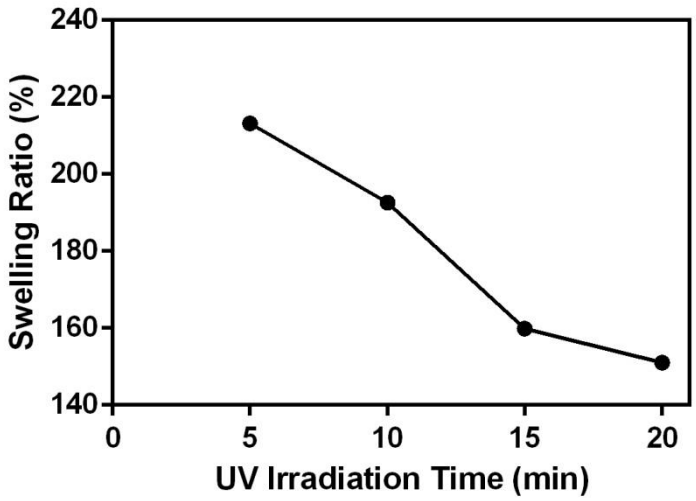

Figure 3.6 Effect of UV irradiation time onto swelling ratio

The hydrogels which were less exposed to the UV light exhibited better water uptake capacity. In other words, swelling ratios of the hydrogels decreases with increasing UV irradiation time, because the increase at UV irridation time increases crosslink density of hydrogel. High crosslink content makes a much denser polymer matrix and so inhibits water absorption. Crosslinker content of the hydrogel is another factor for

swelling behavior of hydrogels. According to the swelling test results, optimum UV time selected as 15 min. Because while hydrogels obtained by using exposure time of 5 or 10 min. were look too soft, hydrogels obtained by using exposure time of 20 min. were rigid resulting in reduction of water absorption capacity of the hydrogel.

3.2 Synthesis of RGO-Based Hydrogel

Firstly, CTS-g-GMA and PEGDA polymer solution was prepared as described above (Section 2.2). In the second step RGO solution was prepared in EtOH and then it sonicated 30 min. to disperse homogeneously RGO in EtOH. RGO solution with four different content was added to polymer solution and exposed to UV light to fabricate RGO-based [(CTS-g-GMA)-PEGDA] hydrogel.

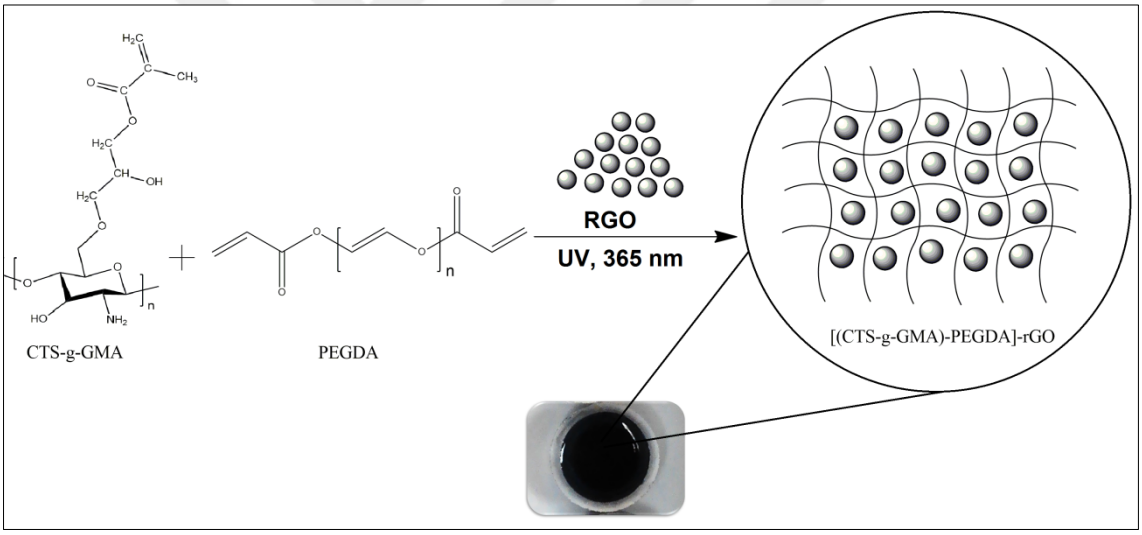

Figure 3.7 Schematic shown of synthesis procedure of RGO-based hydrogel

3.2.1 Characterization of RGO-Based Hydrogel

3.2.1.1 FTIR Analysis

Two weak peaks were observed in the FTIR spectrum of (CTS-g-GMA)-PEGDA at 2960 cm^{-1} and 2920 cm^{-1} which belong to asymmetric and symmetric stretching vibrations of methyl groups in PEGDA. The characteristic band at 1727 cm^{-1} is for the C=O ester stretching of PEGDA. The carbonyl peak appeared more intense in the

Figure 3.7 than other spectrums cause of increasing the number of carbonyl groups with addition of RGO to the hydrogel. The NH bending (Amide II) at 1605 cm^{-1}, representing the presence of newly formed amide bonds between carbonyl groups of RGO and amino groups of the CTS [69]. The absorption band at 1644 cm^{-1} is due to aromatic skeletons in RGO structure.

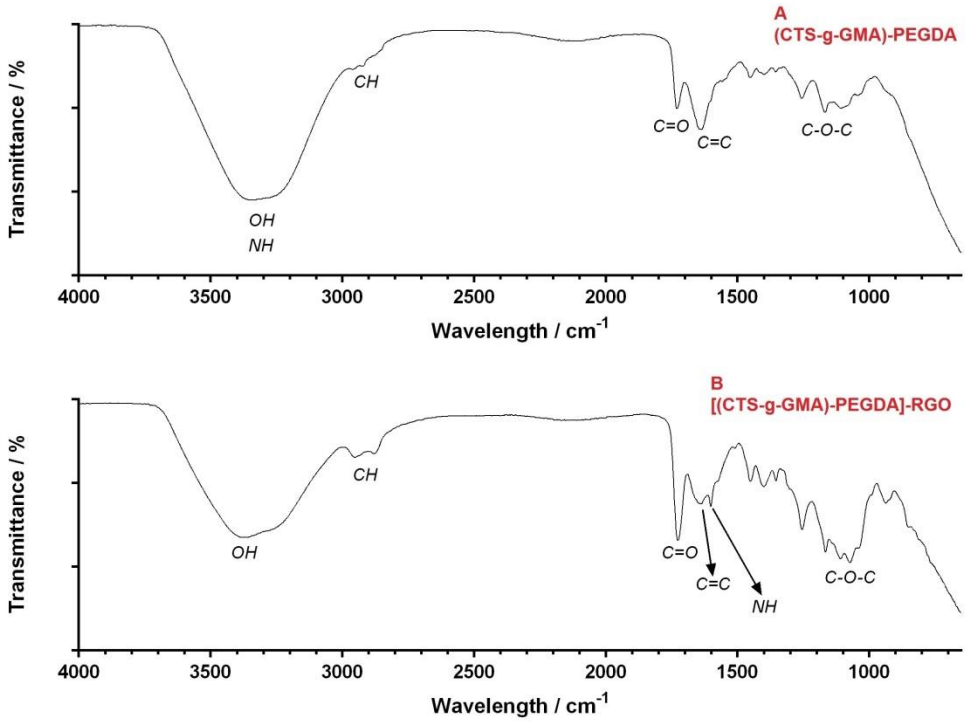

Figure 3.8 FTIR spectrums of (A) (CTS-g-GMA)-PEGDA (B) [(CTS-g-GMA)-PEGDA]-RGO

3.2.1.2 XRD Spectroscopy Analysis

Three peaks observed at $2\theta = 3.33^{o}$, 29.1^{o} and 40.9^{o} in the XRD pattern of (CTS-g-GMA)-PEGDA slightly shifted toward to 3.25^{o}, 27.2^{o} and 42.2^{o} respectively in the XRD spectrum of RGO-based hydrogel.

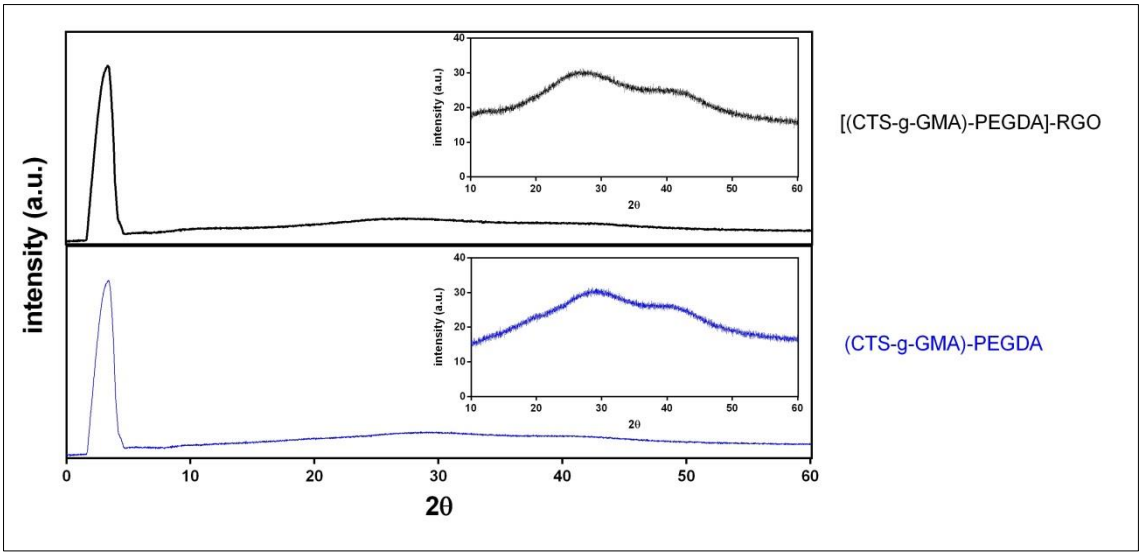

Figure 3.9 XRD spectra of [(CTS-g-GMA)-PEGDA]-RGO and (CTS-g-GMA)-PEGDA

While the both spectra have same trend presenting that good dispersion of RGO particles in the hydrogel network, the shifting of three peaks confirmed the physical and chemical interactions between the functional groups of the hydrogel components and RGO layers.

3.2.2 Thermal Behavior of RGO-Based Hydrogel

The hydrogels w/out RGO exhibited three-stage decomposition in TGA thermographs. In first step, free and bounded water in the hydrogel matrix removed. Second step concerned with decomposition of some oxygen-containing functional groups such as carbonyl and hydroxyl at different positions on w/out RGO based hydrogels [34,52,69]. Last stage decompositions of both TGA graphs are the main weight-loss due to the degradation of crosslinking network. As can be seen from the Figure 3.9, the temperature of the main degradation step was slightly enhanced by incorporation of RGO into the hydrogel matrix (from 427 ^{o}C to 434 ^{o}C)

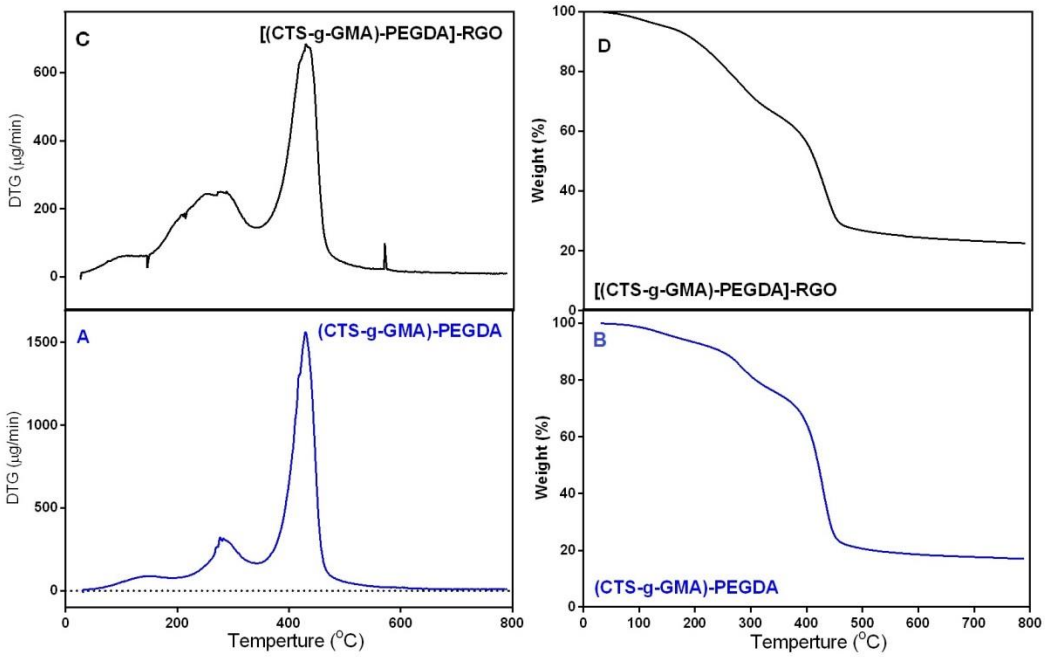

Figure 3.10 DTG and TGA curves of (A and B) (CTS-g-GMA)-PEGDA and (C and D) [(CTS-g-GMA)-PEGDA]-RGO

When temperature increased to 800 °C, a weight loss of 83.33% was observed for (CTS-g-GMA)-PEGDA; on the other hand, [(CTS-g-GMA)-PEGDA]-RGO exhibited weight losses of 77.38%. These differences show fine dispersion of RGO molecules in the network due to the ultrasonic bath of performed polymer solution before the UV photo-crosslinking, stronger interfacial interaction of RGO with hydrogel network, heat barrier effect of RGO molecules and also support the newly formed amide bond between RGO and the hydrogel that was observed the FTIR spectrum [52,53,69].

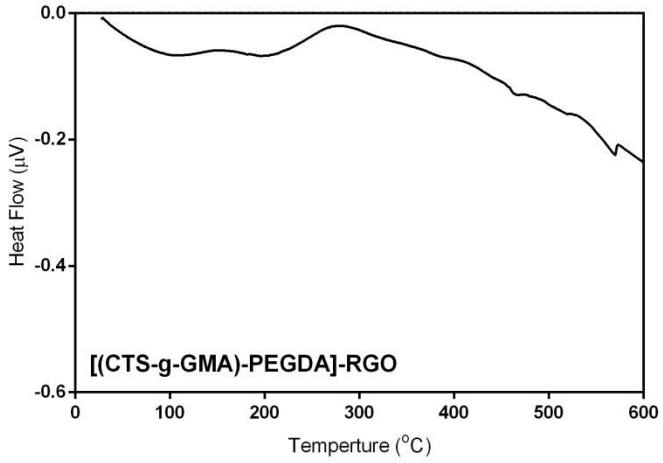

Figure 3.11 DTA curve of [(CTS-g-GMA)-PEGDA]-RGO

In DTA curve, [(CTS-g-GMA)-PEGDA]-RGO showed two endothermic peaks at 101 ^{o}C and 204 ^{o}C which attributed to evaporation of absorbed water and decomposition of oxygen-containing functional groups, respectively. One exothermic peak at 278 ^{o}C was also observed since thermal degradation of polymeric structure.

3.2.3 Cytotoxicity of RGO-Based Hydrogel

Cytotoxicity of the hydrogels was determined by using WST-1 assay and L929 cells seeded onto the hydrogel samples. Polystyrene well was used as control to compare the proliferation of L929 cells. Cytotoxicity test results (Figure 3.12) demonstrate pure and RGO-based hydrogels are biocompatible for the L929 fibroblast cells confirming by one-way ANOVA statistical analyses.

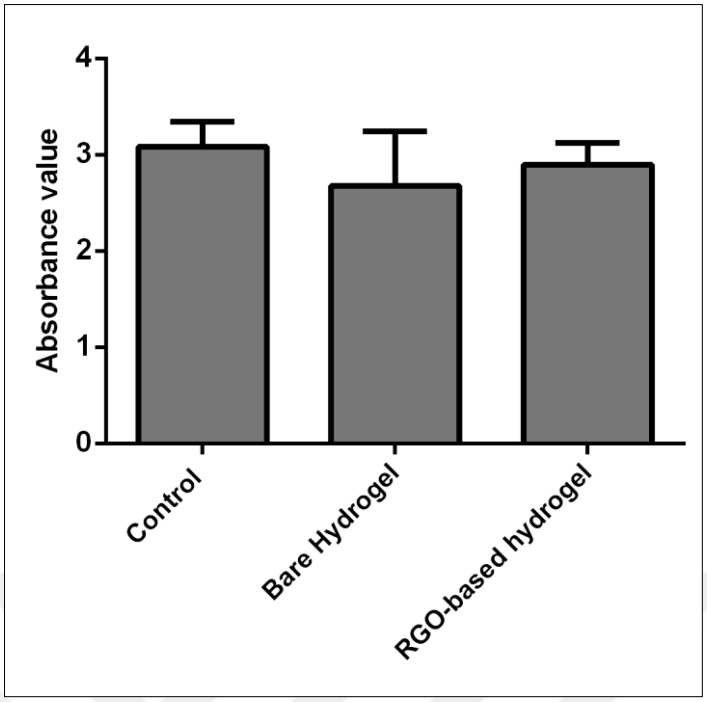

Figure 3.12 Proliferation of L929 cells on the bare hydrogel, RGO-based hydrogel and polystyrene well (control)

3.2.4 Swelling Properties of RGO-Based Hydrogel

Swelling behavior of the RGO-based hydrogels in different weigh ratios were examined by a 24 h swelling test. RGO provided the conductivity to the hydrogel matrix but it had a negative impact on water absorption capacity of the hydrogels. The hydrophilic pendant groups of RGO (OH and COOH) form hydrogen bonds with water molecules and other RGO molecules. On the other hand, carbonyl groups of RGO covalently bonded to amino groups of CTS. As a result of increasing RGO amount in hydrogel matrix, the number of amide bonds between carbonyl groups of RGO and amino group of the CTS increase. These weaken the interaction of hydrophilic pendant groups of RGO with water molecules and hinder the expanding of network. So, swelling capacity of the hydrogels decreases.

The swelling test was not conducted in the case of RGO-based hydrogels including 10-15 % by weight RGO since these hydrogels divided in water. This can be explained that large RGO acted like filler materials and were occurred a steric hindrance against the

water molecules as well as blocked the UV light which causes reducing the photo-crosslink density.

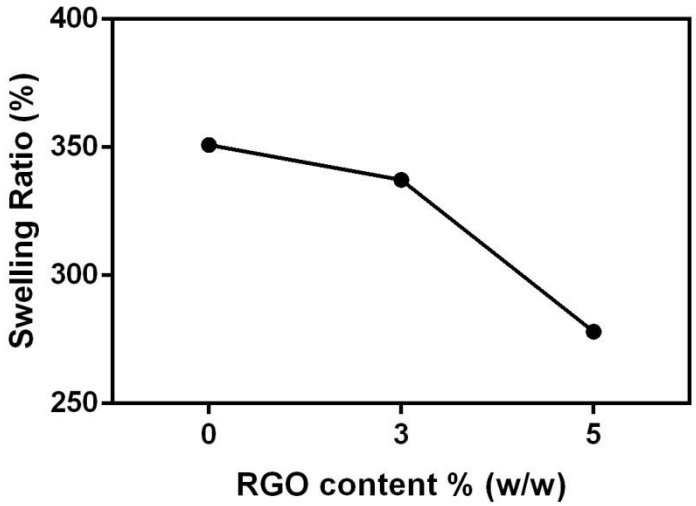

Figure 3.13 Effect of RGO amount onto swelling ratio

3.2.5 Electrical Conductivity of RGO-Based Hydrogels

The RGO-based conductive hydrogels were produced by using four different RGO content as a triplicate (Table 3.1).

Addition of RGO enhanced the electrical conductivity of the hydrogels. RGO molecules were established electron paths in the polymeric network. The RGO molecules are getting closer each other with increasing RGO content of the hydrogel. Thus, electron mobility and conductivity increases until the homogeneous dispersion of RGO molecules disrupt. Despite the increment of RGO amount in hydrogels, the conductivity of [(CTS-g-GMA)-PEGDA]-RGO (15% wt.) is lower than that of [(CTS-g-GMA)-PEGDA]-RGO (10% wt.). When the RGO molecules become too much in the hydrogel network, they may form clusters which cause the losing of homogeneity and eliminate the planar structure. So, electron mobility reduced with increasing RGO content from 10% to 15% by weight.

Table 3.1 Conductivities of RGO-[(CTS-g-GMA)-PEGDA] hydrogels

	Probe Space, s (cm)	Current, I (mA)	Voltage, V (mV)	Sheet Resistivity, ρ (Ω·cm)	Conductivity, σ ($S \cdot cm^{-1}$)	Average Conductivity ($S \cdot cm^{-1}$)
(CTS-g-GMA)-PEGDA	0,127	0,05	NA	NA	NA	NA
[(CTS-g-GMA)-PEGDA]-RGO (3% wt.)	0,127	0,05	54,15	863,76	1,158E-03	1,007E-03
	0,127	0,05	57,78	921,66	1,085E-03	
	0,127	0,05	80,49	1283,91	7,789E-04	
[(CTS-g-GMA)-PEGDA]-RGO (5% wt.)	0,127	0,05	51,43	820,37	1,219E-03	1,370E-03
	0,127	0,05	42,32	675,05	1,481E-03	
	0,127	0,05	44,48	709,51	1,409E-03	
[(CTS-g-GMA)-PEGDA]-RGO (10% wt.)	0,127	0,05	39,70	633,26	1,579E-03	1,716E-03
	0,127	0,05	34,21	545,69	1,833E-03	
	0,127	0,05	36,13	576,32	1,735E-03	
[(CTS-g-GMA)-PEGDA]-RGO (15% wt.)	0,127	0,05	37,00	590,19	1,694E-03	1,366E-03
	0,127	0,05	49,00	781,61	1,279E-03	
	0,127	0,05	55,72	888,80	1,125E-03	

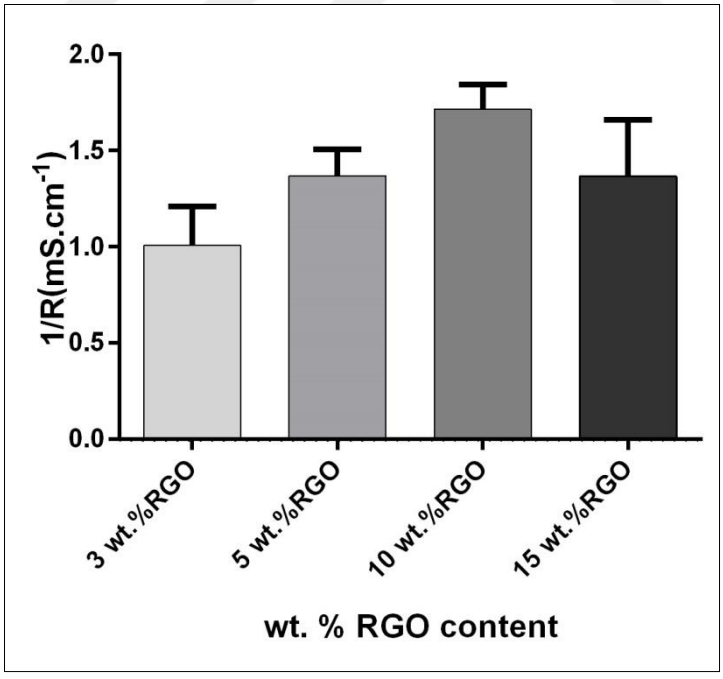

Figure 3.14 Effect of RGO amount onto electrical conductivity

As shown in Table 1, measured the highest average conductivity value is 1.716 x 10^{-3} S/cm. Similar results were obtained for ECHs by other researchers previously. Rebecca A. et al. generated a conductive hydrogel from collagen and single-walled carbon nanotubes (SWNT) which have conductivity of varied from 3 x 10^{-3} to 7 x 10^{-3} S/cm depending on SWNT content [70]. Payam Baei et al. produced electrically conductive gold nanoparticle-CTS thermosensitive hydrogels with a maximum conductivity of ca. 1.3 x 10^{-3} S/cm [27]. In another research, a polyacrylamide/Cu conducting hydrogel was obtained with an electrical conductivity of 1.08 x 10^{-5} S/cm [71]. Jianming Lin et al. also reported a conductivity of 7.3 x 10^{-3} S/cm for a polyacrylate/graphite hydrogel [72]. Another conductive composite hydrogels were prepared from graphene and polyacrylic acid with a conductivity of 1.56 x 10^{-7} S/cm [25].

3.3 Synthesis of PANI-Based Hydrogel

[(CTS-g-GMA)-PEGDA]-PANI hydrogels were fabricated in three different PANI contents. The procedure was demonstrated in the Figure 3.13.

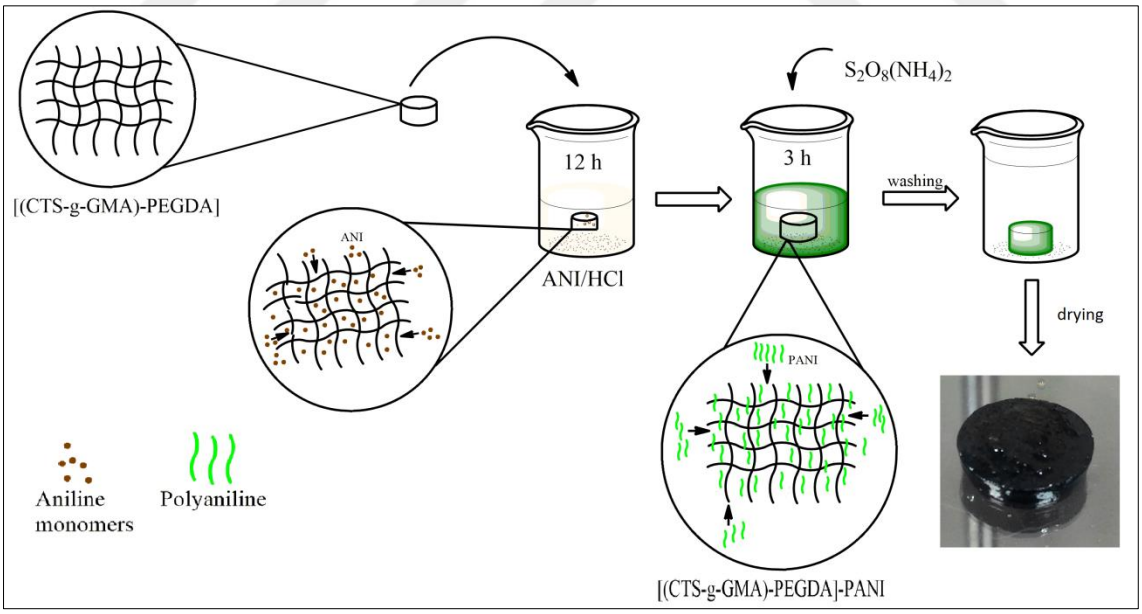

Figure 3.15 Schematic shown of synthesis procedure of PANI-based hydrogel

3.3.1 Characterization of PANI-Based Hydrogel

3.3.1.1 FTIR Spectrocopy Analysis

Figure 3.13-B represents the FTIR spectrum of the [(CTS-g-GMA)-PEGDA]-PANI conductive hydrogel. The stretching vibrations of the O-H and N-H bonds are observed as a wide pike at 3300 cm^{-1}. The vibration band at 1250 cm^{-1} belongs to C–N stretching of the benzenoid structure in polyaniline. The peak appearing at 1457 cm^{-1} is due to N-H bending. Another peak related the presence of polyaniline in hydrogel matrix can be observed at 1613 cm^{-1}, stretching vibrations of C=C bonds.

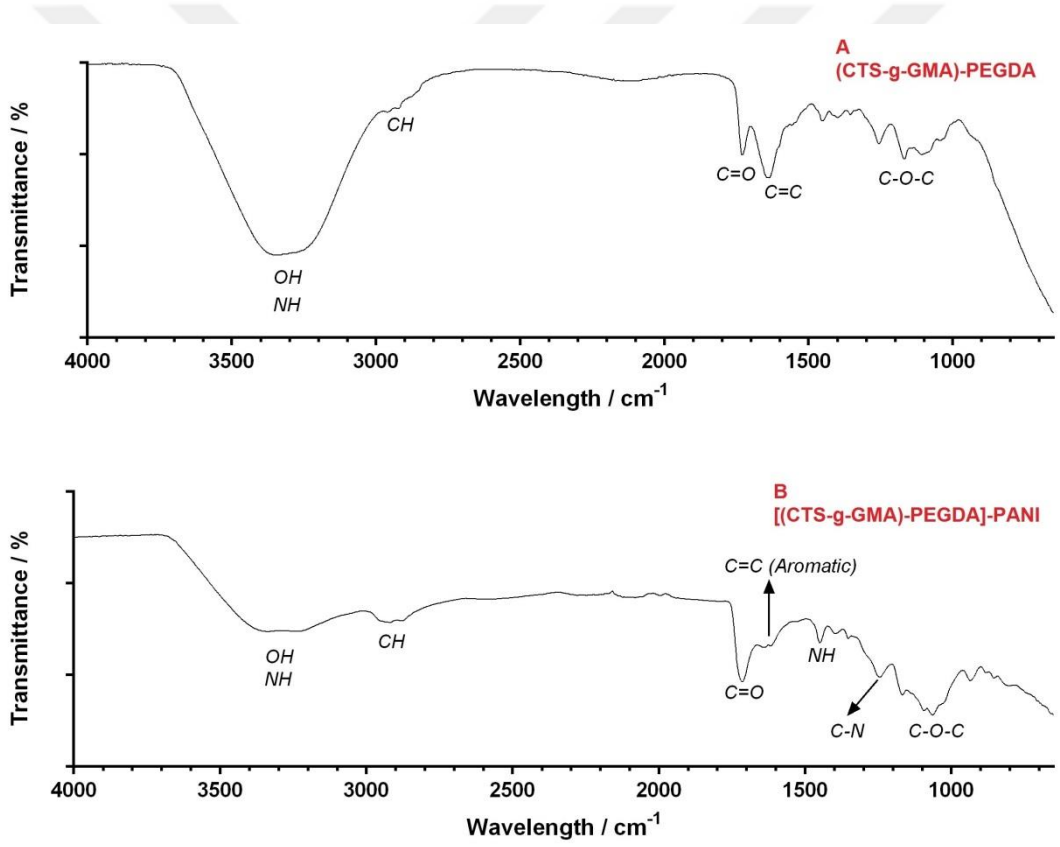

Figure 3.16 FTIR spectrums of (A) (CTS-g-GMA)-PEGDA (B) [(CTS-g-GMA)-PEGDA]-PANI

3.3.1.2 XRD Spectroscopy Analysis

XRD spectra of (CTS-g-GMA)-PEGDA and (CTS-g-GMA)-PEGDA-PANI are shown in Figure 3.15. For hydrogel of (CTS-g-GMA)-PEGDA, three peaks located at 2θ = 3.33°, 29.1° and 40.9°. While the sharp and intense peak (at 3.33°) was assigned to crystalline regions, other two wide peaks (at 29.1° and 40.9°) represented the amorphous regions. As seen from the XRD pattern of PANI contained hydrogel, the wide peak at 29.1° was shifted to 20.8° and also the intensity and sharpness of peak increased compared to that of non-conductive (bare) hydrogel.

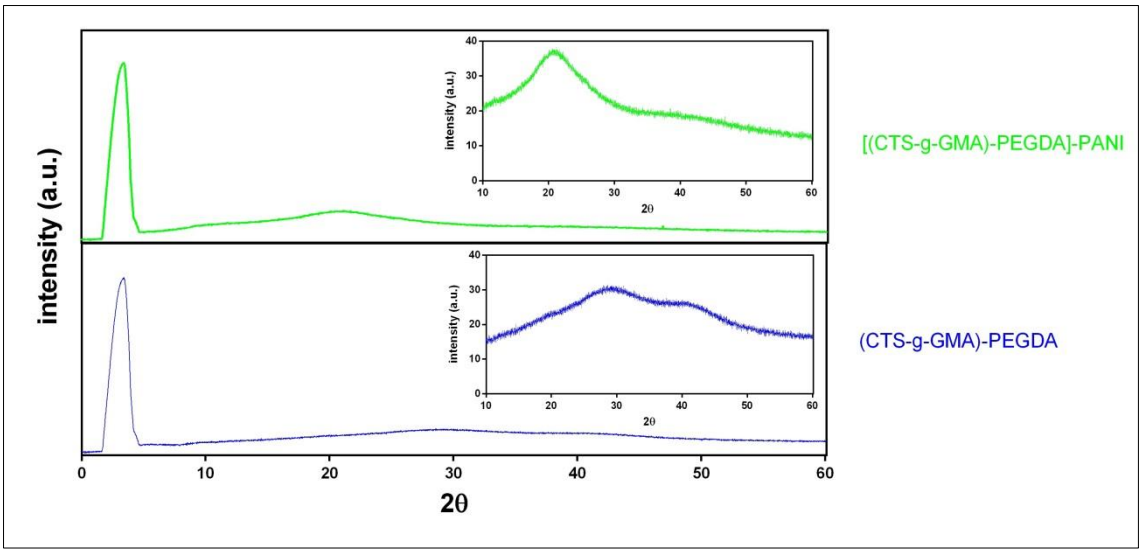

Figure 3.17 XRD spectra of [(CTS-g-GMA)-PEGDA]-PANI and (CTS-g-GMA)-PEGDA

On the other hand, the peak at 40.9° was almost disappeared. These results indicate that the incorporation of PANI was enhanced the crystallinity of hydrogel. The enhancement in crystallinity may be attributed to ordered arrangement and interaction of PANI chains in the hydrogel network.

3.3.2 Thermal Behavior of PANI-Based Hydrogel

TGA curve of the PANI-based conductive hydrogel showed two-stage decomposition. The first stage decomposition of the hydrogel was observed at 202 °C. This can be due to the removal of moisture and dopant material [73]. The main weight-loss region took

place in the temperature range of 310 – 527 ^{o}C which can be due to degradation of semi interpenetrating hydrogel network. While the (CTS-g-GMA)-PEGDA decomposed mainly at 427 ^{o}C, the main decomposition temperature of the conductive hydrogel is 400 ^{o}C. The absorbed PANI into the hydrogel network causes disordered hydrogel network structure leading to lower thermal stability [74,75].

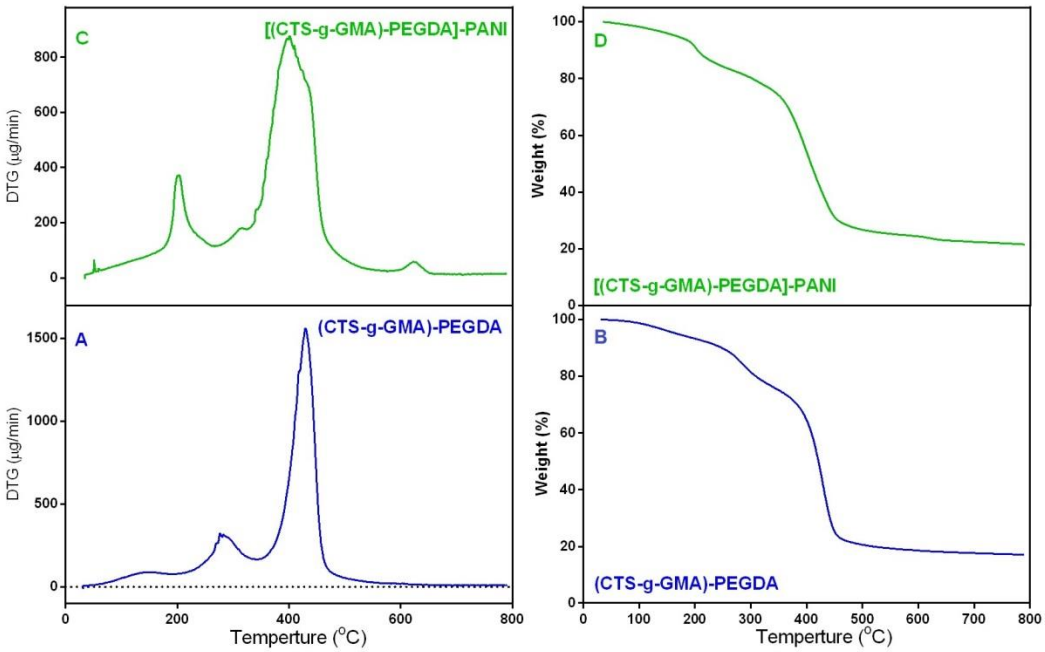

Figure 3.18 DTG and TGA curves of (A and B) (CTS-g-GMA)-PEGDA and (C and D) [(CTS-g-GMA)-PEGDA]-PANI

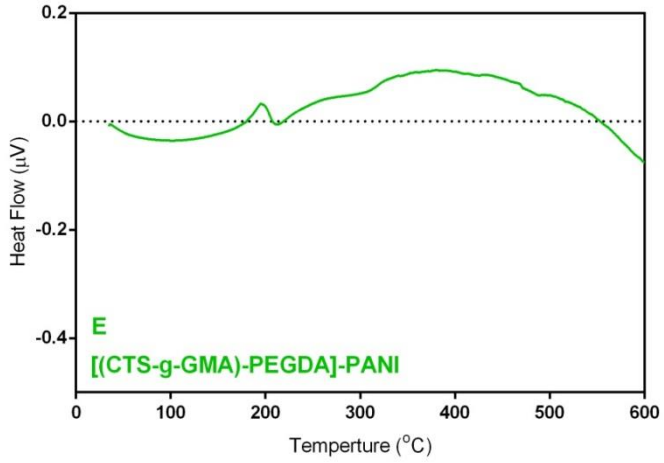

Figure 3.19 DTA curve of [(CTS-g-GMA)-PEGDA]-PANI

In DTA curve, PANI-based hydrogel exhibited one endothermic peak at 105 ^{o}C indicating the water loss in the structure and one wide exothermic peak at 390 ^{o}C corresponding to main degradation of polymeric network.

3.3.3 Cytotoxicity of PANI-Based Hydrogel

Cytotoxicity of the conductive hydrogels was determined by using WST-1 assay. For test, L929 cells were seeded onto the hydrogel samples and polystyrene well. Cytotoxicity test results (Figure 3.20) show that there is no significant difference between the PANI-based hydrogel and control sample indicating pure and PANI-based hydrogel did not cause any cytotoxicity effect on the viability of L929 cells.

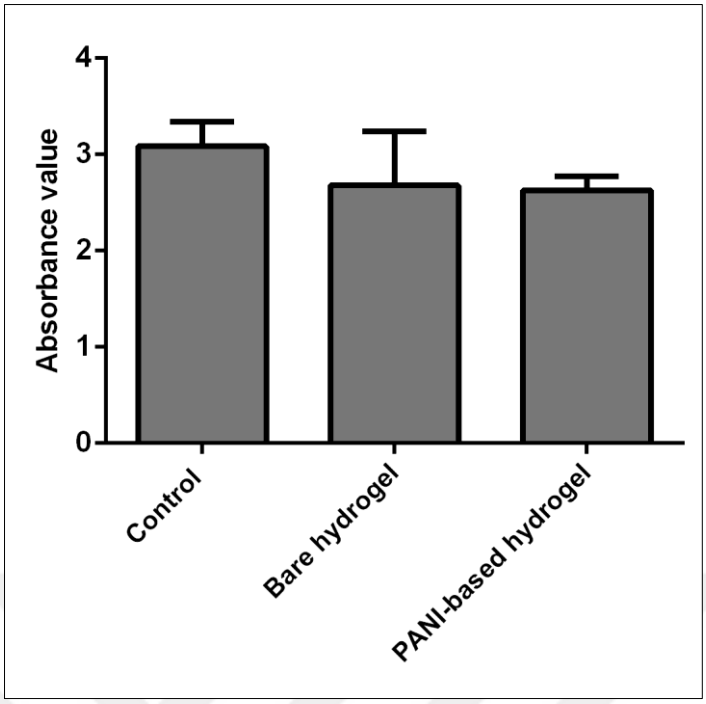

Figure 3.20 Proliferation of L929 cells on the bare hydrogel, PANI-based hydrogel and polystyrene well (control)

3.3.4 Swelling Properties of PANI-Based Hydrogel

The effect of PANI content of the hydrogels on the swelling percentage was investigated. The hydrogels fabricated by the same procedure were immersed in aniline solutions prepared 0.08, 0.16 and 0.32 M monomer concentrations. All other parameters were kept constant. The hydrogel prepared in 0.08M concentration of aniline solution could not stay stable along 24 hours in aqueous medium. At the end of the test, dark green color of small polyaniline pieces ruptured from the hydrogel. Some of polyaniline chains could not hold on to hydrogel network due to the lack of intramolecular interactions (hydrogen bonding). The increase in monomer concentration gave rise to more intramolecular interaction both between polyaniline chains and between polyaniline and hydrogel network. The compact and rigid structure formed as a result of that decreased the swelling capacity. Also, polyaniline chains not only filled the voids in the network but also pore sizes of the hydrogels decreased. So the swelling index of hydrogels decreased with increasing polyaniline amount.

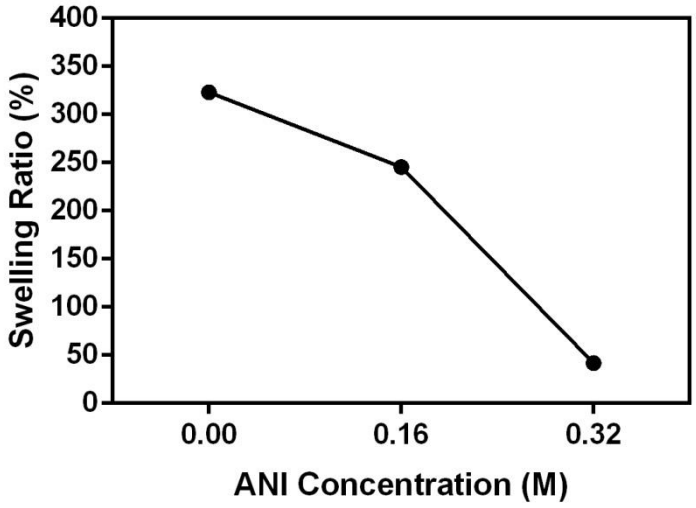

Figure 3.21 Effect of PANI amount onto swelling ratio

3.3.5 Electrical Conductivity of PANI-Based Hydrogels

The obtained pure hydrogels (CTS-g-GMA)-PEGDA immersed solutions at the different concentrations of aniline (0.08, 0.16 and 0.32 M). Entangled PANI chains within the (CTS-g-GMA)-PEGDA network provide the conductivity property to hydrogel as expected.

As shown in Figure 3.19 and listed in Table 3.2 electrical conductivity values increased with increasing PANI loading.

Table 3.2 Conductivities of [(CTS-g-GMA)-PEGDA]-PANI samples

	Probe Space, s (cm)	**Current, I (mA)**	**Voltage, V (mV)**	**Sheet Resistivity, ρ (Ω·cm)**	**Conductivity, σ (S·cm^{-1})**	**Average Conductivity (S·cm^{-1})**
(CTS-g-GMA)-PEGDA	0,127	0,05	NA	NA	NA	NA
[(CTS-g-GMA)-PEGDA]-PANI (0.08M)	0,127	0,05	28,45	453,81	2,204E-03	2,261E-03
	0,127	0,05	32,88	524,48	1,907E-03	
	0,127	0,05	23,46	374,22	2,672E-03	
[(CTS-g-GMA)-PEGDA]-PANI (0.16M)	0,127	0,05	28,88	460,67	2,171E-03	2,363E-03
	0,127	0,05	45,45	724,98	1,379E-03	
	0,127	0,05	17,71	282,50	3,540E-03	
[(CTS-g-GMA)-PEGDA]-PANI (0.32M)	0,127	0,05	10,37	165,41	6,045E-03	7,437E-03
	0,127	0,05	7,982	127,32	7,854E-03	
	0,127	0,05	7,452	118,87	8,413E-03	

The lower conductivity at low PANI concentration is due to the inhomogeneity of PANI chains into the hydrogel matrix. The increment of the conductivity is pretty much at 0.32 M cause of homogeneous layout of PANI chains. Also, disposal of voids inside the hydrogel network by absorption of more PANI polymer chains and crystallinity of PANI enhance the conductivity [76,77]. The increment of the crystallinity after the addition of PANI to the hydrogel was clearly observed XRD spectrum, as well. So, all impacts may be the reasons of the sharp conductivity increase at 0.32 M.

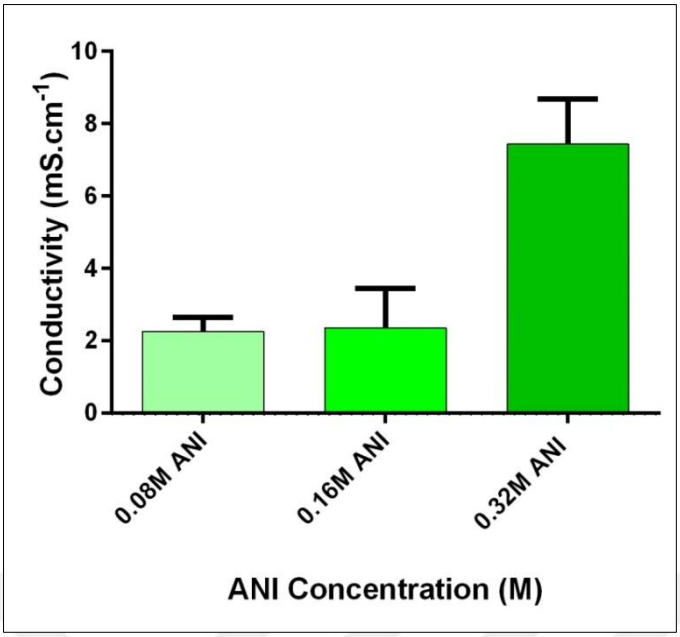

Figure 3.22 Effect of PANI amount onto electrical conductivity

Manufacturing of ECHs by inherently conductive polymers is a very common method. As an example, Nurettin Şahiner and Şahin Demirci produced polyacrylic acid/polyaniline, polyacrylic acid/polythiophene, and polyacrylic acid/polypyrrole cyrogels (a form of hydrogel); the conductivities of them were determined as 2.2 x 10^{-4}, 3.2 x 10^{-4}, and 3.2 x 10^{-3} S/cm, respectively [78]. A 2.69 x 10^{-4} S/cm of conductivity was reported by B.S. Kaith. et al. with gum ghatti-polymethacrylic acid-polyaniline based electrically conductive hydrogel [21]. O-acetyl galacto glucomannan/glycidyl methacrylate/aniline tetramer was synthesized by Weifeng Zhao et al. which have conductivities from 2.93 x 10^{-8} to 1.12 x 10^{-6} S/cm [79]. In another study, an ECH was prepared from polypyrrole and the conductivity of the material was measured as 7.83 x 10^{-3} S/cm [15]. Gusphyl Justin and A. Guiseppi-Elie prepared ECHs in film form as electrode coating materials. The electrical conductivity of the hydrogel-modified electrode was determined as 5.4 x 10^{-5} S/cm [48].

4 CONCLUSIONS

In this study two types of chitosan-based electroconductive hydrogels were fabricated, successfully. One of them was obtained by addition of RGO into the (CTS-g-GMA)-PEGDA hydrogel network. RGO contents of the hydrogels were by weight of 3%, 5%, 10%, and 15%. The presence of carbonyl groups in RGO bonded covalently to amino groups of the CTS in hydrogel matrix was confirmed by FTIR analysis. Encapsulation of RGO into the polymeric structure decreased the swelling capacity of the hydrogels. Thermal analysis showed that RGO-containing hydrogels were more stable thermally than bare hydrogel. According to conductivity measurements; while the conductivities of the hydrogels increases by 10% RGO content, conductivity of hydrogel decreased when used 15% RGO. The highest conductivity (1.716×10^{-3} S/cm) was obtained by encapsulating 10% RGO into the polymeric network ([(CTS-g-GMA)-PEGDA]-RGO).

The other type of electroconductive hydrogel was fabricated by both conversions of aniline monomers to PANI in hydrogel network and absorption of PANI formed in reaction medium into the hydrogel network. The PANI-based semi IPN hydrogels were produced into the aniline solutions of 0.08 M, 0.16 M, and 0.32 M concentrations. According to XRD results the addition of PANI was increased the crystalline regions of the hydrogels. Water uptake capacity of the hydrogels was decreased by increasing PANI content into the hydrogel networks. PANI chains in [(CTS-g-GMA)-PEGDA] reduced the thermal stability of the hydrogels. From the conductivity results, [(CTS-g-GMA)-PEGDA]-PANI (0.32M) has the highest conductivity value which is $7{,}437 \times 10^{-3}$ S/cm.

The superior advantages of fabricated hydrogels in this study such as adjustable swelling capacity owing to photo-crosslinking technique and electrical conductivity provide a potential usage in biomedical fields. These hydrogels may be used as a membrane or coating material for biosensors. Because, they can enhance the sensitivity, detection limit and range of the sensor. These hydrogels also can be modified with a specific enzyme for a biomolecule, thus the hydrogels will be the main component for a biosensor.

REFERENCES

[1] E. M. Ahmed, (2015) Hydrogel: Preparation, characterization, and applications: A review, Journal of Advanced Research, 6(2), 105–121.

[2] A. S. Hoffman, (2012) Hydrogels for biomedical applications, Advanced Drug Delivery Reviews, 64, 18–23.

[3] S. K. . Gulrez, S. Al-Assaf, and G. O. Phillips, (2011) Hydrogels: Methods of Preparation, Characterisation and Applications in Molecular and Environmental Bioengineering, ISBN: 978-953-307-268-5, InTech, 118-150, http://cdn.intechopen.com/pdfs-wm/17237.pdf (17.08.2016).

[4] Q. Vinh, D. Phu, J. Hyung, and D. Sung, (2015) Injectable polymeric hydrogels for the delivery of therapeutic agents : A review, European Polymer Journal, 72, 602–619.

[5] T. R. Hoare and D. S. Kohane, (2008) Hydrogels in drug delivery : Progress and challenges, Polymers with aligned carbon nanotubes: Active composite materials, 49(8), 1993–2007.

[6] W. E. Hennink and C. F. Van Nostrum, (2002) Novel crosslinking methods to design hydrogels, 54, 13–36.

[7] M. F. Akhtar, M. Hanif, and N. M. Ranjha, (2015) Methods of synthesis of hydrogels . . . A review, Saudi Pharmaceutıcal Journal, *"in press"*

[8] G. Ma et al., (2010) Injectable hydrogels based on chitosan derivative/polyethylene glycol dimethacrylate/N,N-dimethylacrylamide as bone tissue engineering matrix, Carbohydrate Polymers, 79(3), 620–627.

[9] N. A. Peppas, J. Z. Hilt, A. Khademhosseini, and R. Langer, (2006) Hydrogels in biology and medicine: From molecular principles to bionanotechnology, Advanced Materials, 18(11), 1345–1360.

[10] K. Y. Lee and D. J. Mooney, (2001) Hydrogels for tissue engineering, Chemical Reviews, 101(7), 1869–1879.

[11] W. Zhao, X. Jin, Y. Cong, Y. Liu, and J. Fu, (2013) Degradable natural polymer hydrogels for articular cartilage tissue engineering, Journal of Chemical

Technology and Biotechnology, 88(3), 327–339.

[12] M. T. Nistor, D. Pamfil, C. Schick, and C. Vasile, (2014) Study of the heat-induced denaturation and water state of hybrid hydrogels based on collagen and poly (N-isopropyl acrylamide) in hydrated conditions, Thermochimica Acta, 589, 114–122.

[13] F. Lee and M. Kurisawa, (2013) Formation and stability of interpenetrating polymer network hydrogels consisting of fibrin and hyaluronic acid for tissue engineering, Acta Biomaterialia, 9(2), 5143–5152.

[14] M. Al-Sibani, A. Al-Harrasi, and R. H. H. Neubert, (2016) Study of the effect of mixing approach on cross-linking efficiency of hyaluronic acid-based hydrogel cross-linked with 1.4 – butandiol diglycidyl ether, European Journal of Pharmaceutical Sciences, 91, 131–137.

[15] X. Liang, B. Qu, J. Li, H. Xiao, B. He, and L. Qian, (2015) Preparation of cellulose-based conductive hydrogels with ionic liquid, Reactive and Functional Polymers, 86, 1–6.

[16] B. J. Kong, A. Kim, and S. N. Park, (2016) Properties and in vitro drug release of hyaluronic acid-hydroxyethyl cellulose hydrogels for transdermal delivery of isoliquiritigenin, Carbohydrate Polymers, 147, 473–481.

[17] M. N. V. R. Kumar, R. a a Muzzarelli, C. Muzzarelli, H. Sashiwa, and a. J. Domb, (2004) Chitosan chemistry and pharmaceutical perspectives, Chemical Reviews, 104(12), 6017–6084.

[18] P. R. Rege and L. H. Block, (1999) Chitosan processing: Influence of process parameters during acidic and alkaline hydrolysis and effect of the processing sequence on the resultant chitosan's properties, Carbohydrate Research, 321(3–4), 235–245.

[19] M. V. Risbud, A. a. Hardikar, S. V. Bhat, and R. R. Bhonde, (2000) pH-sensitive freeze-dried chitosan-polyvinyl pyrrolidone hydrogels as controlled release system for antibiotic delivery, Journal of Controlled Release, 68(1), 23–30.

[20] A. Fatoni, A. Numnuam, P. Kanatharana, W. Limbut, and P. Thavarungkul, (2014) A Conductive Porous Structured Chitosan-grafted Polyaniline Cryogel for

use as a Sialic Acid Biosensor, Electrochimica Acta, 130, 296–304.

[21] B. S. Kaith, K. Sharma, V. Kumar, S. Kalia, and H. C. Swart, (2014) Fabrication and characterization of gum ghatti-polymethacrylic acid based electrically conductive hydrogels, Synthetic Metals, 187(1), 61–67.

[22] Y. Wu et al., (2016) Fabrication of conductive gelatin methacrylate-polyaniline hydrogels, Acta Biomaterialia, 33, 122–130.

[23] C. Chen, C. Yang, S. Li, and D. Li, (2015) A three-dimensionally chitin nanofiber/carbon nanotube hydrogel network for foldable conductive paper, Carbohydrate Polymers, 134, 309–313.

[24] T. Tungkavet, N. Seetapan, D. Pattavarakorn, and A. Sirivat, (2015) Graphene/gelatin hydrogel composites with high storage modulus sensitivity for using as electroactive actuator: Effects of surface area and electric field strength, Polymer, 70, 242–251.

[25] A. Alam et al., (2016) Electrically conductive, mechanically robust, pH-sensitive graphene/polymer composite hydrogels, Composites Science and Technology, 127, 119–126.

[26] G. Sun, B. Li, J. Ran, X. Shen, and H. Tong, (2015) Three-dimensional hierarchical porous carbon/graphene composites derived from graphene oxide-chitosan hydrogels for high performance supercapacitors, Electrochimica Acta, 171, 13–22.

[27] P. Baei, S. Jalili-Firoozinezhad, S. Rajabi-Zeleti, M. Tafazzoli-Shadpour, H. Baharvand, and N. Aghdami, (2016) Electrically conductive gold nanoparticle-chitosan thermosensitive hydrogels for cardiac tissue engineering, Materials Science and Engineering: C, 63, 131–141.

[28] Y. Han et al., (2013) Preparation and electrochemical performances of PEDOT/sulfonic acid-functionalized graphene composite hydrogel, Synthetic Metals, 172, 21–27.

[29] V. Guarino, M. A. Alvarez-Perez, A. Borriello, T. Napolitano, and L. Ambrosio, (2013) Conductive PANi/PEGDA Macroporous Hydrogels For Nerve Regeneration, Advanced Healthcare Materials, 2(1), 218–227.

[30] C. Dispenza, C. Lo Presti, C. Belfiore, G. Spadaro, and S. Piazza, (2006) Electrically conductive hydrogel composites made of polyaniline nanoparticles and poly(N-vinyl-2-pyrrolidone), Polymer, 47(4), 961–971.

[31] R. A. Green, S. Baek, L. A. Poole-Warren, and P. J. Martens, (2010) Conducting polymer-hydrogels for medical electrode applications, Sci Technol Adv Mater Sci Technol Adv Mater, 11(11), 1–13.

[32] T. S. Sreeprasad and V. Berry, (2013) How do the electrical properties of graphene change with its functionalization?, Small, 9(3), 341–350.

[33] M. Ates and a. S. Sarac, (2009) Conducting polymer coated carbon surfaces and biosensor applications, Progress in Organic Coatings, 66, 337–358.

[34] S. Y. Qin, X. J. Liu, R. X. Zhuo, and X. Z. Zhang, (2012) Microstructure-controllable graphene oxide hydrogel film based on a PH-responsive graphene oxide hydrogel, Macromolecular Chemistry and Physics, 213(19), 2044–2051.

[35] Y. Wen, W. Wen, X. Zhang, and S. Wang, (2016) Highly sensitive amperometric biosensor based on electrochemically-reduced graphene oxide-chitosan/hemoglobin nanocomposite for nitromethane determination, Biosensors and Bioelectronics, 79, 894–900.

[36] Y.-F. Bai et al., (2014) Self-assembly of a thin highly reduced graphene oxide film and its high electrocatalytic activity, Nanotechnology, 25(40), 1-9.

[37] V. Singh, D. Joung, L. Zhai, S. Das, S. I. Khondaker, and S. Seal, (2011) Graphene based materials: Past, present and future, Progress in Materials Science, 56(8), 1178–1271.

[38] C. Yu, J. Wang, and Z. M. Liu, (2012) Graphene and its derivative-based biosensing systems, Fenxi Huaxue/ Chinese Journal of Analytical Chemistry, 40(11), 1772–1779.

[39] D. Akyüz, B. Keskin, U. Şahintürk, and A. Koca, (2016) Electrocatalytic hydrogen evolution reaction on reduced graphene oxide electrode decorated with cobaltphthalocyanine, Applied Catalysis B: Environmental, 188, 217–226.

[40] X. Liu, L. Xie, and H. Li, (2012) Electrochemical biosensor based on reduced

graphene oxide and Au nanoparticles entrapped in chitosan/silica sol-gel hybrid membranes for determination of dopamine and uric acid, Journal of Electroanalytical Chemistry, 682, 158–163.

[41] K. Sharma, B. S. Kaith, V. Kumar, S. Kalia, V. Kumar, and H. C. Swart, (2014) Synthesis and biodegradation studies of gamma irradiated electrically conductive hydrogels, Polymer Degradation and Stability, 107, 166–177.

[42] A. Guiseppi-Elie, (2010) Electroconductive hydrogels: Synthesis, characterization and biomedical applications, Biomaterials, 31(10), 2701–2716.

[43] R. Balint, N. J. Cassidy, and S. H. Cartmell, (2014) Conductive polymers: Towards a smart biomaterial for tissue engineering, Acta Biomaterialia, 10(6), 2341–2353.

[44] I. Y. Sapurina and M. a. Shishov, (2012) Oxidative Polymerization of Aniline: Molecular Synthesis of Polyaniline and the Formation of Supramolecular Structures, New Polymers for Special Applications, 251–312.

[45] K. M. Molapo et al., (2012) Electronics of conjugated polymers (I): Polyaniline, International Journal of Electrochemical Science, 7(12), 11859–11875.

[46] P. Humpolicek, V. Kasparkova, P. Saha, and J. Stejskal, (2012) Biocompatibility of polyaniline, Synthetic Metals, 162(7–8), 722–727.

[47] X. Zhao, P. Li, B. Guo, and P. X. Ma, (2015) Antibacterial and conductive injectable hydrogels based on quaternized chitosan-graft-polyaniline/oxidized dextran for tissue engineering, Acta Biomaterialia, 26, 236–248.

[48] G. Justin and A. Guiseppi-Elie, (2009) Characterization of electroconductive blends of poly(HEMA-co-PEGMA-co-HMMA-co-SPMA) and poly(Py-co-PyBA)., Biomacromolecules, 10(9), 2539–2549.

[49] C. N. Kotanen, F. G. Moussy, S. Carrara, and A. Guiseppi-Elie, (2012) Implantable enzyme amperometric biosensors, Biosensors and Bioelectronics, 35(1), 14–26.

[50] C. K. Guiseppi-Elie Anthony, (2010) Development of an implantable biosensor system for physiological status monitoring during long duration space

exploration, Gravitational and Space Research, 23, 55–64.

[51] C. N. Kotanen, C. Tlili, and A. Guiseppi-Elie, (2013) Amperometric glucose biosensor based on electroconductive hydrogels, Talanta, 103, 228–235.

[52] M. Yadav and S. Ahmad, (2015) Montmorillonite/graphene oxide/chitosan composite: Synthesis, characterization and properties, International Journal of Biological Macromolecules, 79, 923–933.

[53] Y. Xiong et al., (2012) Reduced graphene oxide/hydroxylated styrene-butadiene-styrene tri-block copolymer electroconductive nanocomposites: Preparation and properties, Materials Science and Engineering B: Solid-State Materials for Advanced Technology, 177(14), 1157–1163.

[54] J. C. Li, Y. Wang, and D. C. Ba, (2012) Characterization of Semiconductor Surface Conductivity by Using Microscopic Four-Point Probe Technique, Physics Procedia, 32, 347–355.

[55] I. Miccoli, F. Edler, H. Pfnür, and C. Tegenkamp, (2015) The 100th anniversary of the four-point probe technique: the role of probe geometries in isotropic and anisotropic systems, Journal of Physics: Condensed Matter, 27(22), 1-29.

[56] D. M. Stanković, E. Mehmeti, J. Zavašnik, and K. Kalcher, (2016) Determination of nitrite in tap water: A comparative study between cerium, titanium and selenium dioxide doped reduced graphene oxide modified glassy carbon electrodes, Sensors and Actuators B: Chemical, 236, 311–317.

[57] A. Kaya et al., (2016) Reduced graphene oxide based a novel polymer inclusion membrane: Transport studies of Cr(VI), Journal of Molecular Liquids, 219, 1124–1130.

[58] A. T. E. Vilian et al., (2016) Pt-Au bimetallic nanoparticles decorated on reduced graphene oxide as an excellent electrocatalysts for methanol oxidation, Synthetic Metals, 219, 52–59.

[59] W. Zhang et al., (2016) Facile synthesis of binder-free reduced graphene oxide/silicon anode for high-performance lithium ion batteries, Journal of Power Sources, 312, 216–222.

[60] Z. Li et al., (2016) Reduced graphene oxide wrapped MOFs-derived cobalt-doped porous carbon polyhedrons as sulfur immobilizers as cathodes for high performance lithium sulfur batteries, Nano Energy, 23, 15–26.

[61] P. A. Rasheed, T. Radhakrishnan, P. K. Shihabudeen, and N. Sandhyarani, (2016) Reduced graphene oxide-yttria nanocomposite modified electrode for enhancing the sensitivity of electrochemical genosensor, Biosensors and Bioelectronics, 83, 361–367.

[62] T. Thanpitcha, A. Sirivat, A. M. Jamieson, and R. Rujiravanit, (2006) Preparation and characterization of polyaniline/chitosan blend film, Carbohydrate Polymers, 64(4), 560–568.

[63] Y. An et al., (2016) Dual-shell hollow polyaniline/sulfur-core/polyaniline composites improving the capacity and cycle performance of lithium–sulfur batteries, Applied Surface Science, 375, 215–222.

[64] Q. Wu, M. Chen, S. Wang, X. Zhang, L. Huan, and G. Diao, (2016) Preparation of sandwich-like ternary hierarchical nanosheets manganese dioxide/polyaniline/reduced graphene oxide as electrode material for supercapacitor, Chemical Engineering Journal, 304, 29–38.

[65] D. G. Babar, R. Olejnik, P. Slobodian, and J. Matyas, (2016) High sensitivity sensor development for Hexamethylphosphoramide by polyaniline coated polyurethane membrane using resistivity assessment technique, Measurement, 89, 72–77.

[66] N. Hui, X. Sun, Z. Song, S. Niu, and X. Luo, (2016) Gold nanoparticles and polyethylene glycols functionalized conducting polyaniline nanowires for Ultrasensitive and low fouling immunosensing of alpha-fetoprotein, Biosensors and Bioelectronics, 86, 143–149.

[67] A. Khan, S. Badshah, and C. Airoldi, (2011) Biosorption of some toxic metal ions by chitosan modified with glycidylmethacrylate and diethylenetriamine, Chemical Engineering Journal, 171(1), 159–166.

[68] N. Flores-Ramírez et al., (2005) Characterization and degradation of functionalized chitosan with glycidyl methacrylate., Journal of biomaterials

science Polymer edition, 16, 473–488.

[69] J. Wang, G. Zhao, L. Jing, X. Peng, and Y. Li, (2015) Facile self-assembly of magnetite nanoparticles on three-dimensional graphene oxide–chitosan composite for lipase immobilization, Biochemical Engineering Journal, 98, 75–83.

[70] R. A. MacDonald, C. M. Voge, M. Kariolis, and J. P. Stegemann, (2008) Carbon nanotubes increase the electrical conductivity of fibroblast-seeded collagen hydrogels, Acta Biomaterialia, 4(6), 1583–1592.

[71] J. Lin, Q. Tang, and J. Wu, (2007) The synthesis and electrical conductivity of a polyacrylamide/Cu conducting hydrogel, Reactive and Functional Polymers, 67(6), 489–494.

[72] J. Lin, Q. Tang, J. Wu, and S. Hao, (2007) The synthesis and electrical conductivity of a polyacrylate/graphite hydrogel, Reactive and Functional Polymers, 67(4), 275–281.

[73] P. Varakirkkulchai, S. Kongparakul, and P. Prasassarakich, (2015) Polyaniline/polyacrylate core-shell composites: Preparation, morphology and anticorrosive properties, Progress in Organic Coatings, 85, 84–91.

[74] Y. Jia, J. Jiang, and K. Sun, (2015) Pyrolysis of polyaniline-poly(styrene sulfonate) hydrogels to prepare activated carbons for the adsorption of vitamin B12, Journal of Analytical and Applied Pyrolysis, 111, 247–253.

[75] M. Park, D. Lee, S. Shin, H. J. Kim, and J. Hyun, (2016) Flexible conductive nanocellulose combined with silicon nanoparticles and polyaniline, Carbohydrate Polymers, 140, 43–50.

[76] Y. Xia, J. M. Wiesinger, A. G. MacDiarmid, and A. J. Epstein, (1995) Camphorsulfonic Acid Fully Doped Polyaniline Emeraldine Salt: Conformations in Different Solvents Studied by an Ultraviolet/Visible/Near-Infrared Spectroscopic Method, Chemistry of Materials, 7(3), 443–445.

[77] D. Zhang, (2007) On the conductivity measurement of polyaniline pellets, Polymer Testing, 26(1), 9–13.

[78] N. Sahiner and S. Demirci, (2016) Conducting semi-interpenetrating polymeric composites via the preparation of poly(aniline), poly(thiophene), and poly(pyrrole) polymers within superporous poly(acrylic acid) cryogels, Reactive and Functional Polymers, 105, 60–65.

[79] W. Zhao, L. Glavas, K. Odelius, U. Edlund, and A. C. Albertsson, (2014) A robust pathway to electrically conductive hemicellulose hydrogels with high and controllable swelling behavior, Polymer (United Kingdom), 55(13), 2967–2976.

ÖZGEÇMİŞ

Kişisel Bilgiler

Adı Soyadı: Celil ULUTÜRK

Adress: Fındıklı Mh. Serin Sk. No: 70/9 Maltepe - İSTANBUL

Doğum Yeri ve Tarihi: İstanbul / 05.08.1989

Email: celilulutrk@gmail.com

Eğitim Bilgileri

2003 – 2007 Şenesenevler Lisesi, Süper Lise (İngilizce)

2007 – 2012 Bülent Ecevit Üniversitesi, Fen-Edebiyat Fakültesi, Kimya Bölümü

2013 – Marmara Üniversitesi, Fen Bilimleri Enstitüsü, Kimya Müh. Bölümü